

Central exclusive quark-antiquark dijet and Standard Model Higgs boson production in proton-(anti)proton collisions

Rafał Maciuła*

Institute of Nuclear Physics PAN, PL-31-342 Cracow, Poland

Roman Pasechnik†

*Department of Physics and Astronomy,
Uppsala University, Box 516, SE-751 20 Uppsala, Sweden*

Antoni Szczurek‡

*Institute of Nuclear Physics PAN, PL-31-342 Cracow, Poland and
University of Rzeszów, PL-35-959 Rzeszów, Poland*

(Dated: November 6, 2018)

Abstract

We consider the central exclusive production of $q\bar{q}$ pairs and Higgs boson in proton-proton collisions at LHC. The amplitude for the process is derived within the k_{\perp} -factorization approach and considered in different kinematical asymptotics, in particular, in the important high quark transverse momenta and massless quark limits. Quark helicity and spin-projection amplitudes in two different frames are shown in extenso. Rapidity distributions, quark jet p_{\perp} distributions, invariant $q\bar{q}$ mass distributions, angular azimuthal correlations between outgoing protons and jets are presented. Irreducible $b\bar{b}$ background to the central exclusive Higgs boson production is analyzed in detail, in particular how to impose cuts to maximize signal-to-background ratio.

PACS numbers: 13.87.Ce,14.65.Dw

*Electronic address: rafal.maciula@ifj.edu.pl

†Electronic address: roman.pasechnik@fysast.uu.se

‡Electronic address: antoni.szczurek@ifj.edu.pl

I. INTRODUCTION

Exclusive double diffractive production (EDD) of the Higgs boson has been suggested some time ago as alternative to inclusive measurements [1, 2]. Exclusive diffractive dijets production attracted recently a lot of attention due to new data from CDF run II [3]. The standard approach for the calculation of central dijets production in proton-(anti)proton collisions is based on the Kaidalov-Khoze-Martin-Ryskin (KKMR) QCD mechanism which was initially developed for the central exclusive Higgs production in Refs. [4] which is expected to provide a really robust signal due to a clean environment and highly suppressed backgrounds (see, e.g. Refs. [5–7]). For more details on the central exclusive processes and related physics, we refer to the most recent reviews in Ref. [8].

It is known, however, that the process $pp \rightarrow pp(q\bar{q})$ is dominated by the non-perturbative region of gluon transverse momenta, and even perturbative ingredients like the Sudakov form factor are not under full theoretical control [9]. Uncertainties on exclusive diffractive production of Higgs at the LHC were discussed in Ref. [10] together with uncertainties on gluonic jet production which was measured by the CDF collaboration. The problem becomes even more pronounced when considering the irreducible backgrounds in central exclusive production of Higgs boson originating from the direct exclusive $b\bar{b}$ pair production in a fusion of two off-shell gluons. In particular, in Ref. [11] it was shown that the central exclusive production (CEP) of $b\bar{b}$ jets at LHC (see Fig. 1), may totally shadow the corresponding signal of the Higgs boson in the $b\bar{b}$ channel (see Fig. 2), which may lead to significant problems in experimental identification.

Therefore, it becomes very important to investigate the exclusive quark jets production in different kinematical domains and quantify the related theoretical uncertainties. On the other hand, the analysis of various differential distributions and experimental cuts in considered four-body reaction $pp \rightarrow p + \text{“gap”} + (q\bar{q}) + \text{“gap”} + p$ could help in a reduction of the corresponding backgrounds.

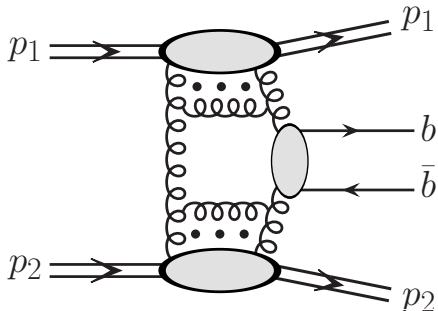


FIG. 1: Direct central exclusive $b\bar{b}$ pair production in k_{\perp} -factorization approach. It is considered to be the main irreducible background for Higgs CEP.

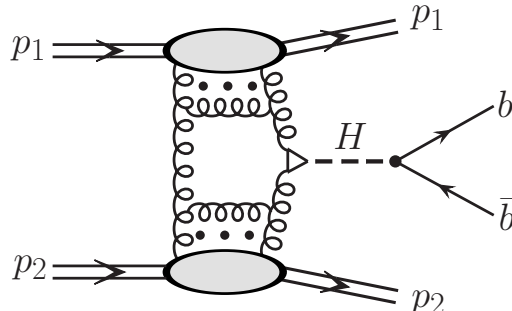


FIG. 2: Central exclusive production of Higgs boson production with its subsequent decay into $b\bar{b}$ pair, which competes with the direct $b\bar{b}$ pair production shown in Fig. 1.

Unpolarized exclusive c and \bar{c} jets production was investigated numerically in Ref. [12]. It was found that the whole process is dominated by quark/antiquark production with low transverse momentum k_{\perp} in the very forward limit of outgoing protons, whereas it is strongly suppressed at high k_{\perp} 's, much stronger than in inclusive case. The same should hold for b and \bar{b} jets CEP, which constitutes the major part of the irreducible background

for central exclusive Higgs production¹. As was demonstrated numerically in Ref. [11], such a background turned out to be dominated by small gluon transverse momenta $\sim q_\perp$ (which are the same for both active and screening gluons in the forward limit) coming into hard subprocess amplitude $g^*g^* \rightarrow q\bar{q}$ contracted with the gluon transverse polarization vectors $\sim q_\perp^\mu/x\sqrt{s}$ and integrated over in the diffractive amplitude. The presence of the screening gluon in the loop, actually, violates the well known $J_z = 0$ selection rule [14], which was initially established in one-step mechanisms, like $\gamma^*\gamma^*$ and PP fusion processes. Such a violation manifests itself in the fact that the hard subprocess amplitude is non-zero and proportional to gluon transverse momentum, and it is indeed strongly suppressed only in the high quark transverse momentum limit, whereas in the low- k_\perp limit it may lead to a significant contribution [11, 12].

These observations still suffer from a lack of solid theoretical background. In order to predict observable signal from quark dijets at LHC and to make a decisive conclusion about irreducible background for Higgs CEP, it is worth to analyze carefully different kinematical limits both numerically and analytically. The main goal of this paper is to derive explicitly the hard subprocess amplitude $g^*g^* \rightarrow q\bar{q}$ for any quark helicity states λ_q and $\lambda_{\bar{q}}$ in diffractive kinematics in two different configurations of large $k_\perp \gg m_q$ and small $k_\perp \ll m_q$ quark transverse momenta focusing primarily on large invariant mass of $q\bar{q}$ dijets. This would give us an opportunity to analyze different kinematical asymptotics of the diffractive amplitude. Having such amplitudes we can then numerically evaluate differential distributions in quark transverse momenta, rapidity, relative angle between the quark jets and invariant mass of the $q\bar{q}$ dijet. These theoretical elements are necessary for upcoming Higgs searches and diffractive dijets measurements at LHC.

In the present paper we extend earlier studies related to Higgs and jet production [4, 9, 15] to the production of quark-antiquark jets. In our approach we use unintegrated gluon distributions as proposed by the Durham group [4]. Slightly different gluon distributions, fitted to the HERA data, have been used in Ref. [9]. The choice of gluon distributions brings uncertainties of a factor of about 2. In our case we consistently use the same gluon distributions for the signal and background. In the case of Higgs production we shall use off-shell matrix element for $g^*g^* \rightarrow H$ compared to the on-shell matrix element used before.

The paper is organized as follows. In Section II we consider the general kinematics of the central exclusive dijet production. Section III is devoted to a discussion of the diffractive amplitude, in particular, its hard and soft constituents. Explicit derivation of the helicity amplitudes for the hard subprocess part $g^*g^* \rightarrow q\bar{q}$ in general kinematics and in some important limits is given in Section IV. Electromagnetic $\gamma^*\gamma^*$ contribution is discussed in Section V. In Section VI we reexamine the central Higgs production taking into account gluon virtualities and explore contributions of the exclusive $b\bar{b}$ pair and Z production as backgrounds for Higgs. Section VII contains discussion of numerical results. Finally, some concluding remarks and outlook are given in Section VIII.

II. KINEMATICS OF THE CENTRAL EXCLUSIVE DIJET PRODUCTION

Inclusive heavy quark/antiquark pair production in the framework of the k_\perp -factorization approach [16] was considered in detail in Refs. [17–19]. In particular, it was shown

¹ Other backgrounds although in principle irreducible can be large [13].

that the combination of the k_{\perp} -factorization approach and the next-to-leading-logarithmic-approximation (NLLA) BFKL vertex in Quasi-multi-Regge kinematics (QMRK) [20] together with the concept of unintegrated gluon distribution functions (UGDFs) gives quite good agreement with data on inclusive heavy $q\bar{q}$ pair production.

It looks quite natural to apply similar ideas to exclusive diffractive $q\bar{q}$ production in proton-(anti)proton collisions at different energies. In Figs. 3 and 4 we show the general kinematics for the process $pp \rightarrow p + \text{“gap”} + (q\bar{q}) + \text{“gap”} + p$ under consideration at the parton and the hadron levels, respectively.

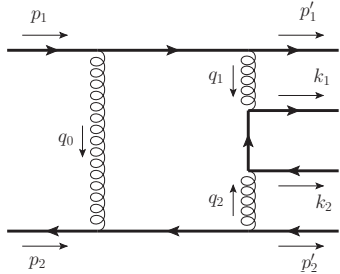


FIG. 3: General kinematics of exclusive diffractive $q\bar{q}$ pair production in pp collisions at the parton level.

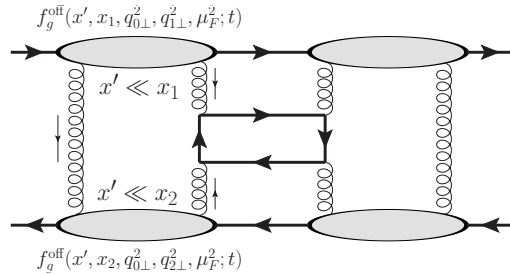


FIG. 4: Cross section of $2 \rightarrow 4$ process of exclusive diffractive $q\bar{q}$ pair production at the hadron level.

The decomposition of gluon momenta into longitudinal and transverse parts in the high energy limit in the c.m.s. frame is

$$\begin{aligned} q_1 &= x_1 p_1 + q_{1\perp}, & q_2 &= x_2 p_2 + q_{2\perp}, & 0 < x_{1,2} < 1, \\ q_0 &= x'_1 p_1 + x'_2 p_2 + q_{0\perp}, & x'_1 \sim x'_2 = x' &\ll x_{1,2}, & q_{0,1,2}^2 \simeq q_{0/1/2\perp}^2. \end{aligned} \quad (2.1)$$

Making use of conservation laws

$$q_1 = p_1 - p'_1 - q_0, \quad q_2 = p_2 - p'_2 + q_0, \quad q_1 + q_2 = k_1 + k_2, \quad (2.2)$$

we write

$$s x_1 x_2 = M_{q\bar{q}}^2 + |\mathbf{k}_{\perp}|^2 \equiv M_{q\bar{q}\perp}^2, \quad M_{q\bar{q}}^2 = (k_1 + k_2)^2, \quad x_{1,2} = \frac{M_{q\bar{q}\perp}}{\sqrt{s}} e^{\pm y_{q\bar{q}}}, \quad (2.3)$$

where $M_{q\bar{q}}$ and $y_{q\bar{q}}$ is the invariant mass and rapidity of the $q\bar{q}$ pair, respectively, and

$$k_{\perp} = -(p'_{1\perp} + p'_{2\perp}) = q_{1\perp} + q_{2\perp} = k_{1\perp} + k_{2\perp},$$

is its transverse momentum, where $q_{1/2\perp}$ and $k_{1/2\perp}$ are gluon and quark transverse momenta with respect to the c.m.s. beam axis. In analogy with Eq. (2.1), we can write

$$p'_1 = \xi_1 p_1 + p'_{1\perp}, \quad p'_2 = \xi_2 p_2 + p'_{2\perp}, \quad \xi_{1,2} = 1 - x_{1,2}, \quad (2.4)$$

where $p'^2_{1/2\perp} = t_{1,2}$ in terms of the momentum transfers along the proton lines $t_{1,2}$.

In the c.m.s. frame it is convenient to choose the basis with z -axis collinear to the proton beam. Then the proton momenta are

$$p_1 = \frac{\sqrt{s}}{2}(1, 0, 0, 1), \quad p_2 = \frac{\sqrt{s}}{2}(1, 0, 0, -1). \quad (2.5)$$

Let us choose the y -axis in such a way that $q_1^y = -q_2^y \equiv q^y$. In these coordinates the gluon transverse momenta are

$$q_{1\perp} = (0, q_1^x, q^y, 0), \quad q_{2\perp} = (0, q_2^x, -q^y, 0). \quad (2.6)$$

Conservation laws provide us with the following relations between components of gluon transverse momenta and covariant scalar products

$$\begin{aligned} q_1^x &= -\frac{q_{1\perp}^2 + (q_{1\perp}q_{2\perp})}{|\mathbf{k}_\perp|}, \quad q_2^x = -\frac{q_{2\perp}^2 + (q_{1\perp}q_{2\perp})}{|\mathbf{k}_\perp|}, \quad q^y = \frac{\sqrt{q_{1\perp}^2 q_{2\perp}^2 - (q_{1\perp}q_{2\perp})^2}}{|\mathbf{k}_\perp|} \text{sign}(q^y), \\ k_\perp^2 &= -|\mathbf{k}_\perp|^2 = q_{1\perp}^2 + q_{2\perp}^2 + 2(q_{1\perp}q_{2\perp}), \quad q_{1/2\perp}^2 = -|\mathbf{q}_{1/2\perp}|^2, \end{aligned} \quad (2.7)$$

where $|\mathbf{k}_\perp|$ is the $q\bar{q}$ -pair transverse momentum with respect to z -axis. On the other hand, momentum conservation $\mathbf{p}'_{1\perp} + \mathbf{p}'_{2\perp} = \mathbf{k}_\perp$ leads to a useful relation

$$-t_1 - t_2 + 2\sqrt{t_1 t_2} \cos \Phi = |\mathbf{k}_\perp|, \quad (2.8)$$

where Φ is the relative angle between the outgoing protons.

The appearance of the factor $\text{sign}(q^y)$ guarantees the applicability of Eq. (2.7) for both positive and negative q^y . Note that under permutations $q_{1\perp} \leftrightarrow q_{2\perp}$ implied by the Bose statistics the components interchange as $q_1^x \leftrightarrow q_2^x$ and $q^y \leftrightarrow -q^y$.

In analogy to Eq. (2.1) one can introduce the Sudakov expansions for quark momenta as

$$k_1 = x_1^q p_1 + x_2^q p_2 + k_{1\perp}, \quad k_2 = x_1^{\bar{q}} p_1 + x_2^{\bar{q}} p_2 + k_{2\perp} \quad (2.9)$$

leading to

$$x_{1,2} = x_{1,2}^q + x_{1,2}^{\bar{q}}, \quad x_{1,2}^q = \frac{m_{1\perp}}{\sqrt{s}} e^{\pm y_1}, \quad x_{1,2}^{\bar{q}} = \frac{m_{2\perp}}{\sqrt{s}} e^{\pm y_2}, \quad m_{1/2\perp}^2 = m_q^2 + |\mathbf{k}_{1/2\perp}|^2, \quad (2.10)$$

in terms of quark/antiquark rapidities y_1, y_2 and transverse masses $m_{1\perp}, m_{2\perp}$. In the considered coordinates we write in analogy to Eq. (2.6)

$$k_{1\perp} = (0, k_1^x, k^y, 0), \quad k_{2\perp} = (0, k_2^x, -k^y, 0), \quad (2.11)$$

with components satisfying the relation $k_1^x + k_2^x = q_1^x + q_2^x$. By construction, in order to get the diffractive amplitude in the covariant form useful in any coordinates, we should relate components $k_{1/2}^x$ and k^y with the scalar products in the similar way as for gluon momentum components (see Eq. (2.7)):

$$k_1^x = -\frac{k_{1\perp}^2 + (k_{1\perp}k_{2\perp})}{|\mathbf{k}_\perp|}, \quad k_2^x = -\frac{k_{2\perp}^2 + (k_{1\perp}k_{2\perp})}{|\mathbf{k}_\perp|}, \quad k^y = \frac{\sqrt{k_{1\perp}^2 k_{2\perp}^2 - (k_{1\perp}k_{2\perp})^2}}{|\mathbf{k}_\perp|} \text{sign}(k^y). \quad (2.12)$$

In subsequent calculations we will construct the $q\bar{q}$ diffractive amplitude in explicitly covariant form and analyze its behavior in different regions of the 4-particle phase space.

III. DIFFRACTIVE AMPLITUDE

Generally, in the case of the central exclusive production (CEP) with the leading protons, the central system X should necessarily be produced in the color singlet state, such that the proton remnants and the X system are disconnected in the color space and their hadronisation occurs independently giving rise to rapidity gaps [21]. So, without the loss of generality we are concentrated on the simplest case of $q\bar{q}$ pair produced in the color singlet state.

According to the KKMR approach [4–7] we write the amplitude of the exclusive diffractive $q\bar{q}$ pair production $pp \rightarrow p(q\bar{q})p$ as

$$\mathcal{M}_{\lambda_q \lambda_{\bar{q}}} = s \cdot \pi^2 \frac{1}{2} \frac{\delta_{c_1 c_2}}{N_c^2 - 1} \Im \int d^2 q_{0\perp} V_{\lambda_q \lambda_{\bar{q}}}^{c_1 c_2} \frac{f_g^{\text{off}}(x', x_1, q_{0\perp}^2, q_{1\perp}^2, t_1) f_g^{\text{off}}(x', x_2, q_{0\perp}^2, q_{2\perp}^2, t_2)}{q_{0\perp}^2 q_{1\perp}^2 q_{2\perp}^2}, \quad (3.1)$$

where the transverse momenta and the longitudinal fractions of gluons are defined in the previous Section, $\lambda_q, \lambda_{\bar{q}}$ are the helicities of heavy q and \bar{q} , respectively, f_g^{off} is the unintegrated gluon density function (UGDF) and $V_{\lambda_q \lambda_{\bar{q}}}^{c_1 c_2}$ is the hard subprocess $g^* g^* \rightarrow b\bar{b}$ amplitude. Averaging over color indices c_1, c_2 of t -channel fusing gluons is made explicitly. The normalization convention of this amplitude differs from the KKMR one by a factor s . The amplitude is averaged over the color indices and over the two transverse polarizations of the incoming gluons. The bare amplitude above is subjected to absorption corrections which depend on collision energy and typical proton transverse momenta. We shall discuss this issue shortly when presenting our results.

A. Matrix element of the hard subprocess $g^* g^* \rightarrow Q\bar{Q}$

Let us consider the subprocess amplitude for the $q\bar{q}$ pair production via off-shell gluon-gluon fusion. The vertex factor $V_{\lambda_q \lambda_{\bar{q}}}^{c_1 c_2} = V_{\lambda_q \lambda_{\bar{q}}}^{c_1 c_2}(k_1, k_2)$ in expression (3.1) is the production amplitude of a pair of massive quark q and antiquark \bar{q} with helicities $\lambda_q, \lambda_{\bar{q}}$ and momenta k_1, k_2 , respectively. Within the QMRK approach [20] we have

$$V_{\lambda_q \lambda_{\bar{q}}}^{c_1 c_2}(q_1, q_2) \equiv n_\mu^+ n_\nu^- V_{\lambda_q \lambda_{\bar{q}}}^{c_1 c_2, \mu\nu}(q_1, q_2), \quad n_\mu^\mp = \frac{p_{1,2}^\mu}{E_{p, cms}}, \quad (3.2)$$

$$V_{\lambda_q \lambda_{\bar{q}}}^{c_1 c_2, \mu\nu}(q_1, q_2) = -g^2 \sum_{i,k} \langle 3i, \bar{3}k | 1 \rangle \bar{u}_{\lambda_q}(k_1) (t_{ij}^{c_1} t_{jk}^{c_2} b^{\mu\nu}(k_1, k_2) - t_{kj}^{c_2} t_{ji}^{c_1} \bar{b}^{\mu\nu}(k_2, k_1)) v_{\lambda_{\bar{q}}}(k_2),$$

where $E_{p, cms} = \sqrt{s}/2$ is the c.m.s. proton energy, t^c are the color group generators in the fundamental representation, $u(k_1)$ and $v(k_2)$ are on-shell quark and antiquark spinors, respectively, $b^{\mu\nu}, \bar{b}^{\mu\nu}$ are the effective vertices (3.3) arising from the Feynman rules in the QMRK approach illustrated in Fig. 5:

$$b^{\mu\nu}(k_1, k_2) = \gamma^\nu \frac{\hat{q}_1 - \hat{k}_1 - m_q}{(q_1 - k_1)^2 - m_q^2} \gamma^\mu - \frac{\gamma_\beta \Gamma^{\mu\nu\beta}(q_1, q_2)}{(k_1 + k_2)^2}, \quad (3.3)$$

$$\bar{b}^{\mu\nu}(k_2, k_1) = \gamma^\mu \frac{\hat{q}_1 - \hat{k}_2 + m_q}{(q_1 - k_2)^2 - m_q^2} \gamma^\nu - \frac{\gamma_\beta \Gamma^{\mu\nu\beta}(q_1, q_2)}{(k_1 + k_2)^2},$$

where by the Dirac convention $\hat{a} \equiv \gamma \cdot a$ for any 4-vector a^μ is adopted, $\Gamma^{\mu\nu\beta}(q_1, q_2)$ is the effective three-gluon vertex. These effective vertices were initially proposed for massless

quarks in Refs. [20] and then extended for massive case in Ref. [17, 22]. The effective ggg -vertices are canceled out when projecting the $q\bar{q}$ production amplitude Eq. (3.2) onto the color singlet state, so only the first two diagrams in Fig. 5 contribute to the final result for the production amplitude. Since we will adopt the definition of gluon polarization vectors proportional to transverse momenta $q_{1/2\perp}$, i.e. $\varepsilon_{1,2} \sim q_{1/2\perp}/x_{1,2}$ (see below), then we take into account the longitudinal momenta in the numerators of effective vertices (3.3).

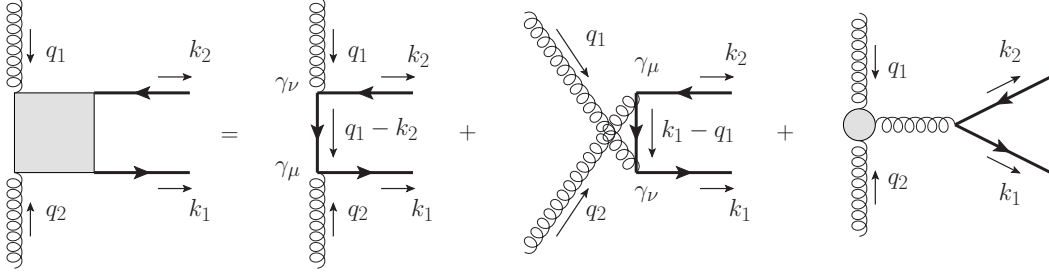


FIG. 5: Effective vertex in QMRK approach [20]. Last diagram with effective 3-gluon vertex drops out in projection to the color singlet final state.

The SU(3) Clebsch-Gordan coefficient $\langle 3i, \bar{3}k | 1 \rangle = \delta^{ik}/\sqrt{N_c}$ in Eq. (3.2) projects out the color quantum numbers of the $q\bar{q}$ pair onto the color singlet state. Factor $1/\sqrt{N_c}$ provides the averaging of the matrix element squared over intermediate color states of quarks.

Therefore, we have the following amplitude

$$V_{\lambda_q \lambda_{\bar{q}}}^{c_1 c_2, \mu\nu} = -\frac{g^2}{2\sqrt{N_c}} \delta^{c_1 c_2} \bar{u}_{\lambda_q}(k_1) \left(\gamma^\nu \frac{\hat{q}_1 - \hat{k}_1 - m_q}{(q_1 - k_1)^2 - m_q^2} \gamma^\mu - \gamma^\mu \frac{\hat{q}_1 - \hat{k}_2 + m_q}{(q_1 - k_2)^2 - m_q^2} \gamma^\nu \right) v_{\lambda_{\bar{q}}}(k_2). \quad (3.4)$$

This amplitude can be simplified by using Dirac equations for quark/antiquark spinors

$$\bar{u}_{\lambda_q}(k_1) \hat{k}_1 = m_q \bar{u}_{\lambda_q}(k_1), \quad \hat{k}_2 v_{\lambda_{\bar{q}}}(k_2) = -m_q v_{\lambda_{\bar{q}}}(k_2), \quad k_1^2 = k_2^2 = m_q^2. \quad (3.5)$$

Moving \hat{k}_1 to the left, and \hat{k}_2 to the right, until they disappear upon acting on the spinor, we finally get

$$V_{\lambda_q \lambda_{\bar{q}}, \mu\nu}^{c_1 c_2} = -\frac{g^2}{2\sqrt{N_c}} \delta^{c_1 c_2} \bar{u}_{\lambda_q}(k_1) \left(\frac{\gamma^\nu \hat{q}_1 - 2k_1^\nu}{q_1^2 - 2(k_1 q_1)} \gamma^\mu - \gamma^\mu \frac{\hat{q}_1 \gamma^\nu - 2k_2^\nu}{q_1^2 - 2(k_2 q_1)} \right) v_{\lambda_{\bar{q}}}(k_2). \quad (3.6)$$

Amplitude of fusion of two off-shell (reggeized) gluons $g^* g^* \rightarrow q\bar{q}$ turns out to be explicitly gauge invariant. Indeed, by direct calculation we see that the gauge invariance over the first gluon line is satisfied:

$$q_1^\nu V_{\lambda_q \lambda_{\bar{q}}, \mu\nu}^{c_1 c_2} = 0. \quad (3.7)$$

Now due to momentum conservation $q_1 + q_2 = k_1 + k_2$ we may rewrite the amplitude (3.4) as follows

$$V_{\lambda_q \lambda_{\bar{q}}, \mu\nu}^{c_1 c_2} = \frac{g^2}{2\sqrt{N_c}} \delta^{c_1 c_2} \bar{u}_{\lambda_q}(k_1) \left(\gamma^\nu \frac{\hat{q}_2 \gamma^\mu - 2k_2^\mu}{q_2^2 - 2(k_2 q_2)} - \frac{\gamma^\mu \hat{q}_2 - 2k_1^\mu}{q_2^2 - 2(k_1 q_2)} \gamma^\nu \right) v_{\lambda_{\bar{q}}}(k_2). \quad (3.8)$$

Thus, the gauge invariance over the second gluon line is also satisfied:

$$q_2^\mu V_{\lambda_q \lambda_{\bar{q}}, \mu\nu}^{c_1 c_2} = 0. \quad (3.9)$$

Comparing Eqs. (3.6) and (3.8) we see that the amplitude is symmetric w.r.t. interchanges $q_1 \leftrightarrow q_2$ and $\mu \leftrightarrow \nu$ as it should be.

Taking into account definition (3.2) and momentum conservation (2.1) and using the gauge invariance properties (3.7) and (3.9), we get the following projection to the light cone vectors (so called ‘‘Gribov’s trick’’)

$$V_{\lambda_q \lambda_{\bar{q}}}^{c_1 c_2} = n_\mu^+ n_\nu^- V_{\lambda_q \lambda_{\bar{q}}, \mu\nu}^{c_1 c_2} = \frac{4}{s} \frac{q_1^\nu - q_{1\perp}^\nu}{x_1} \frac{q_2^\mu - q_{2\perp}^\mu}{x_2} V_{\lambda_q \lambda_{\bar{q}}, \mu\nu}^{c_1 c_2} = \frac{4}{s} \frac{q_{1\perp}^\nu}{x_1} \frac{q_{2\perp}^\mu}{x_2} V_{\lambda_q \lambda_{\bar{q}}, \mu\nu}^{c_1 c_2}. \quad (3.10)$$

Last expression shows that an important consequence of the gauge invariance is the vanishing of the matrix element of the effective $ggq\bar{q}$ -vertex between on-mass-shell quark and antiquark states in the limit of small $q_{1\perp}$ and $q_{2\perp}$ [17, 22]

$$V_{\lambda_q \lambda_{\bar{q}}}^{c_1 c_2} \rightarrow 0 \quad \text{for} \quad q_{1\perp} \text{ or } q_{2\perp} \rightarrow 0, \quad (3.11)$$

The normalization of polarization vectors coincides with that of Ref. [23]. Now using Eqs. (2.3), (3.10) and (3.3) we finally get the following $q\bar{q}$ production vertex

$$V_{\lambda_q \lambda_{\bar{q}}}^{c_1 c_2} = -\frac{2g^2}{M_{q\bar{q}\perp}^2 \sqrt{N_c}} \delta^{c_1 c_2} \bar{u}_{\lambda_q}(k_1) \left(\frac{\hat{q}_{1\perp} \hat{q}_1 - 2(k_{1\perp} q_{1\perp})}{q_{1\perp}^2 - 2(k_1 q_1)} \hat{q}_{2\perp} - \hat{q}_{2\perp} \frac{\hat{q}_1 \hat{q}_{1\perp} - 2(k_{2\perp} q_{1\perp})}{q_{1\perp}^2 - 2(k_2 q_1)} \right) v_{\lambda_{\bar{q}}}(k_2). \quad (3.12)$$

It is interesting to note that this vertex function would be equal to zero if one substitutes $q_1 \rightarrow q_{1\perp}$, i.e. when one neglects the longitudinal components of gluon momenta $q_{1/2,\perp}$ putting $x_1 \rightarrow 0$ or $x_2 \rightarrow 0$. So, it turns out that the longitudinal momenta play a critical role in diffractive production of $q\bar{q}$ pair and cannot be neglected. At the same time, we keep the gluon virtualities in the propagators in Eq. (3.12) as they apparently become important in the small quark masses and quark transverse momenta.

It is worth to notice that the mass terms disappear when applying the Dirac equations (3.5). The quark mass m_q is present in the spinors and in the scalar products only. So, we see that for massless quarks the production amplitude (3.12) has the same covariant form as for massive ones.

In both particular cases of $\mathbf{p}'_{1\perp} = -\mathbf{p}'_{2\perp}$ and in the forward limit $|\mathbf{p}'_{1\perp}| = |\mathbf{p}'_{2\perp}| \rightarrow 0$, we have $q_{1\perp} = -q_{2\perp} \equiv q_\perp$ and, hence, $k_{1\perp} = -k_{2\perp} \equiv k_\perp$. High- k_\perp jets limit corresponds to $m_q \ll k_\perp$ and $q_\perp \ll k_\perp$. Invariant mass of the $q\bar{q}$ pair is then given by $M_{q\bar{q}}^2 \simeq 4|\mathbf{k}_\perp|^2$, and the calculation of the matrix element squared $|V(q_1, q_2)|^2$ for the considered hard subprocess (3.12) in this limit leads to

$$\sum_{\lambda_q \lambda_{\bar{q}}} |V_{\lambda_q \lambda_{\bar{q}}}|^2 \simeq \frac{8g^4}{N_c} \left(\frac{q_\perp}{k_\perp} \right)^4 \sin^2(2\phi), \quad (3.13)$$

where ϕ is the relative angle between \mathbf{k}_\perp and \mathbf{q}_\perp vectors. We see now that the amplitude (3.12) in the high- k_\perp limit is not exactly zero, but rather suppressed by a factor $\sim q_\perp^2/k_\perp^2$. However, relation (3.13) cannot be used for prediction of the corresponding high- k_\perp asymptotics of the diffractive amplitude (3.1) since it contains the hard subprocess amplitude $V(q_1, q_2)$ in the first power integrated over q_\perp . For this purpose we have to consider initial expression (3.12) for particular quark helicity configurations separately paying attention not only at their asymptotical behavior, but also at symmetry w.r.t. $\mathbf{q}_\perp \leftrightarrow -\mathbf{q}_\perp$. Large- k_\perp behavior of the 4-particle phase space is important as well.

B. $Q\bar{Q}$ center of mass helicity amplitudes for the hard subprocess $g^*g^* \rightarrow Q\bar{Q}$

Let us consider now separate quark/antiquark helicity contributions of the off-shell gluon fusion (hard) subprocess $g^*g^* \rightarrow Q_{\lambda_q}\bar{Q}_{\lambda_{\bar{q}}}$, given by the matrix element in the general covariant form (3.12).

The most convenient way is to determine the quark/antiquark helicities in the c.m.s. frame of the $Q\bar{Q}$ pair with z axis along the proton beam, so $\mathbf{k}_1 = -\mathbf{k}_2$ and $k_{1,2}^0 = M_{q\bar{q}}/2$. For simplicity, we work in the limit of forward scattering, so $p'_{1\perp} = p'_{2\perp} = 0$, so $\mathbf{q}_{1\perp} = -\mathbf{q}_{2\perp} = \mathbf{q}_{0\perp}$. In this frame momenta of protons and final-state quarks are

$$\begin{aligned} p_1^\mu &= \frac{E_1}{\sqrt{2}}(1, 0, 0, 1), & p_2^\mu &= \frac{E_2}{\sqrt{2}}(1, 0, 0, -1), \\ k_1^\mu &= E_q(1, \gamma \sin \theta_q \cos \varkappa, \gamma \sin \theta_q \sin \varkappa, \gamma \cos \theta_q), & \gamma &= \frac{\sqrt{E_q^2 - m_q^2}}{E_q} < 1, \\ k_2^\mu &= E_q(1, -\gamma \sin \theta_q \cos \varkappa, -\gamma \sin \theta_q \sin \varkappa, -\gamma \cos \theta_q), \end{aligned}$$

so that the proton and quark energies $E_{1,2}$, E_q and the polar angle of a (anti)quark jet θ_q w.r.t. the z -axis are defined as

$$\begin{aligned} E_q &\equiv \frac{M_{q\bar{q}}}{2} = \frac{E_1}{\sqrt{2}}(x_1^q + x_1^{\bar{q}}) = \frac{E_2}{\sqrt{2}}(x_2^q + x_2^{\bar{q}}), \\ \cos \theta_q &= \frac{1}{\gamma} \frac{x_1^q - x_1^{\bar{q}}}{x_1^q + x_1^{\bar{q}}}, & \sin \theta_q &= \frac{1}{\gamma} \frac{\sqrt{\gamma^2(x_1^q + x_1^{\bar{q}})^2 - (x_1^q - x_1^{\bar{q}})^2}}{x_1^q + x_1^{\bar{q}}}, \end{aligned}$$

where $x_{1,2}^{q,\bar{q}}$ are the Sudakov fractions defined in Eq. (2.10). The gluon and quark transverse momenta (with respect to the proton beam) in the polar coordinates are then defined as

$$\mathbf{q}_{0\perp} = q_\perp(\cos \psi, \sin \psi), \quad \mathbf{k}_{1\perp} = -\mathbf{k}_{2\perp} = k_\perp(\cos \varkappa, \sin \varkappa),$$

respectively, and

$$k_\perp = E_q \frac{\sqrt{\gamma^2(x_1^q + x_1^{\bar{q}})^2 - (x_1^q - x_1^{\bar{q}})^2}}{x_1^q + x_1^{\bar{q}}}, \quad k_z = E_q \frac{x_1^q - x_1^{\bar{q}}}{x_1^q + x_1^{\bar{q}}}, \quad |\mathbf{k}| = \sqrt{k_\perp^2 + k_z^2} = E_q \gamma. \quad (3.14)$$

Using these notations, the different helicity amplitudes $V_{\lambda_q \lambda_{\bar{q}}}$ can be written as follows:

$$\begin{aligned} V_{+-} &= \mathcal{C} \frac{q_\perp^2}{|\mathbf{k}|} \left[2|\mathbf{k}|q_\perp \left(|\mathbf{k}| \cos(\psi - \varkappa) - ik_z \sin(\psi - \varkappa) \right) + M_{q\bar{q}}k_\perp \left(k_z \cos(2\psi - 2\varkappa) - \right. \right. \\ & \left. \left. i|\mathbf{k}| \sin(2\psi - 2\varkappa) \right) \right] / \left[M_{q\bar{q}}^2(k_\perp^2 + q_\perp^2 + m_q^2) + 4M_{q\bar{q}}k_\perp q_\perp k_z \cos(\psi - \varkappa) - \right. \\ & \left. 2k_\perp^2 q_\perp^2 (1 + \cos(2\psi - 2\varkappa)) + q_\perp^4 \right], \end{aligned} \quad (3.15)$$

$$\begin{aligned} V_{++} &= -2\mathcal{C} e^{-i\varkappa} \frac{q_\perp^2 m_q}{|\mathbf{k}|} \left[k_\perp^2 \cos(2\psi - 2\varkappa) + |\mathbf{k}|^2 \right] / \left[M_{q\bar{q}}^2(k_\perp^2 + q_\perp^2 + m_q^2) + \right. \\ & \left. 4M_{q\bar{q}}k_\perp q_\perp k_z \cos(\psi - \varkappa) - 2k_\perp^2 q_\perp^2 (1 + \cos(2\psi - 2\varkappa)) + q_\perp^4 \right] \end{aligned} \quad (3.16)$$

with normalisation $\mathcal{C} = 2g^2\delta^{c_1c_2}/\sqrt{N_c}$. Up to a phase factor, the helicity amplitudes are dependent on the difference $\psi - \varkappa$ (coming from the scalar product $(\mathbf{k}_\perp \mathbf{q}_{0\perp})$) and thus explicitly invariant with respect to rotations of \mathbf{k}_\perp and $\mathbf{q}_{0\perp}$ in the transverse plane or shifts of the angles $\psi, \varkappa \rightarrow \psi + \delta, \varkappa + \delta$.

Covariant relations (3.14) allow us to turn to any desirable frame of reference, in particular, to the overall c.m.s. frame, where the (anti)quark longitudinal momentum fractions $x_{1,2}^{q,\bar{q}}$ are defined through their rapidities y_1, y_2 in Eq. (2.10) and the $q\bar{q}$ invariant mass is given by

$$M_{q\bar{q}} = \sqrt{2m_\perp^2(1 + \cosh(y_1 - y_2))}. \quad (3.17)$$

Let us now investigate the hard subprocess $g^*g^* \rightarrow q\bar{q}$ matrix elements (3.15) and (3.16) in two limits of high and low- k_\perp jets separately.

Physically interesting case is for $q\bar{q}$ dijets with very high invariant mass $M_{q\bar{q}} \gg m_q$, where the KKMR QCD mechanism [4] based on the k_\perp -factorization and Sudakov evolution is strictly justified. If one looks at centrally produced jets $y_{1,2} \rightarrow 0$, then according to Eq. (3.17) the only way to produce the large invariant mass $M_{q\bar{q}}$ is to consider high- k_\perp jets limit $|k_\perp| \gg m_q, |q_\perp|$. As follows from Eq. (3.14), such a limit corresponds to the quark and antiquark at central rapidities $y_{1,2} \sim 0$, $x_1^q \sim x_1^{\bar{q}}$ and the $q\bar{q}$ invariant mass $M_{q\bar{q}} \simeq 2k_\perp$.

We see from Eqs. (3.16) that $V_{++} \rightarrow 0$ in the quark massless limit $m_q \rightarrow 0$ as it should be, so it is generally suppressed with respect to V_{+-} in the limit of large invariant mass $M_{q\bar{q}}$ and high- k_\perp quarks, i.e. for $M_{q\bar{q}}, k_\perp \gg m_q, q_\perp$. Indeed, in high- k_\perp quarks limit, the helicity amplitudes are

$$V_{+-} \simeq -i\mathcal{C} \frac{q_\perp^2}{2k_\perp^2} \sin(2\psi - 2\varkappa), \quad V_{++} \simeq -\mathcal{C} e^{-i\varkappa} \frac{q_\perp^2 m_q}{2k_\perp^3} (1 + \cos(2\psi - 2\varkappa)). \quad (3.18)$$

Then summing up the non-zero contributions $|V_{\lambda_q \lambda_{\bar{q}}}|^2$ we easily recover Eq. (3.13) for unpolarized hard matrix element squared in the considered limit. However, V_{+-} actually drops out in the integration over ψ in the diffractive amplitude due to antisymmetry with respect to the interchange $\psi \leftrightarrow -\psi$. So the diffractive cross section for the $q\bar{q}$ pair production is given by V_{++} contribution only and gets significantly suppressed in the high- k_\perp limit by a factor $\sim q_\perp^2 m_q / k_\perp^3$. So, in this case quark masses m_q and off-forward corrections become important. This is in agreement with the common belief that the Higgs CEP background is supposed to be small in very forward and quark massless limits for centrally produced $b\bar{b}$ jets (with small rapidities), and agrees well with the $J_z = 0$ selection rule [14].

However, the particular high- k_\perp limit does not explain the whole story. Observation we have made above means only that quark high- k_\perp contributions in the central rapidity region may be strongly suppressed with respect to low- k_\perp jets, where the gluon transverse momenta q_\perp and quark masses are significant, but it does not tell us that the whole $b\bar{b}$ background for Higgs production is suppressed.

In our previous analysis of the exclusive open charm production in Ref. [12] it was shown that the dominant contribution to the $c\bar{c}$ dijet cross section comes from relatively small quark transverse momenta $|k_\perp| \simeq 1$ GeV. The same should hold for $b\bar{b}$ CEP relevant for the Higgs background. Indeed, resolving relation (3.17) with respect to typical rapidity difference $|y_1 - y_2| = \Delta y$, neglecting quark transverse momenta $|k_\perp| \ll m_q$ and keeping only the b -mass contributions $m_b \simeq 4.5$ GeV at fixed $M_{q\bar{q}} \sim M_H = 120$ GeV, we get $\Delta y \simeq 6.6$, $x_1^q \gg x_1^{\bar{q}}$. So the low- k_\perp quark jets can provide a contribution to irreducible

background for Higgs CEP, if their rapidities are $y_{1,2} \simeq \pm 3.3$. Then the invariant mass of the quark/antiquark pair is given by their longitudinal fractions (or rapidities) only

$$M_{q\bar{q}} \simeq 2m_q \sqrt{\cosh(y_1) \cosh(y_2)}, \quad |y_{1,2}| \gg 1. \quad (3.19)$$

In the last kinematical situation the helicity amplitudes (3.15), (3.16) are not suppressed by a large denominator, and significant contributions can be obtained. Indeed,

$$V_{+-} \simeq \frac{\mathcal{C} e^{i(z-\psi)}}{2\sqrt{\cosh(y_1) \cosh(y_2)}} \frac{q_\perp^3}{m_q(m_q^2 + q_\perp^2)}, \quad V_{++} \simeq \frac{-\mathcal{C} e^{-iz}}{2\sqrt{\cosh(y_1) \cosh(y_2)}} \frac{q_\perp^2}{m_q^2 + q_\perp^2} \quad (3.20)$$

which in the considered limit $q_\perp \sim k_\perp \ll m_q$ up to a common phase factor coincide with our previously published result in Ref. [11]. Again, analogously to the previous case V_{+-} drops out in the integration over ψ in the diffractive amplitude. The leading symmetric w.r.t. $\psi \leftrightarrow -\psi$ contribution to V_{+-}

$$V_{+-}^{sym} \sim \frac{q_\perp^4 k_\perp}{M_{q\bar{q}} m_q^4} \ll V_{++}$$

is again extremely suppressed w.r.t. V_{++} in the considered low- k_\perp asymptotics.

Numerically, dominant low- k_\perp contribution coming from V_{++} amplitude (of course, at not extremely large $y_{1,2}$) in the case of b -jets can lead to a dominant contribution to the exclusive background for the Higgs CEP. In this asymptotics, the quark mass m_q plays an important role since it comes into the denominator in Eq. (3.20). Precise evaluation of the corresponding signal, however, demands employing the formulae for the hard amplitudes in the general form given by Eqs. (3.15) and (3.16). Detailed numerical investigation of contributions from different parts of the phase space will be presented below in the Results section.

C. Unintegrated gluon distributions

In our approach we use unintegrated gluon distributions as proposed by Khoze, Martin and Ryskin (see e.g. [4]). In Ref. [9] slightly different unintegrated gluon distributions taken from the analysis of Ivanov and Nikolaev [24] were used. These gluon distributions have been adjusted to the deep-inelastic HERA data. In addition the authors have shown that their off-diagonal UGDFs provide a good description of the Tevatron data on exclusive dijet production [9]. The KMR UGDFs discussed in the present paper also reasonably well describe the dijet data [10, 25].

Let us now consider in detail the couplings of gluons to protons. At the parton level, we assume that hard active gluons (carrying the momentum fractions $x_{1,2}$) and screening gluons (carrying the momentum fraction $x' \ll x_{1,2}$) couple to a quark line in the proton in the normal way. In order to turn to the hadron level, the factor $C_F \alpha_s(\mu_{\text{soft}}^2)/\pi$ [23] is absorbed into the off-diagonal unintegrated gluon distribution function (UGDF) $f_g^{\text{off}}(x', x_{1,2}, q_{1/2\perp}^2, q_{0\perp}^2, \mu_F^2; t)$. The absorbed coupling $\alpha_s(\mu_{\text{soft}}^2)$ corresponds to the coupling of the screening gluon with virtuality $\mu_{\text{soft}}^2 \sim q_{0\perp}^2$ to a quark in the proton, whereas the coupling of the active gluons to the $q\bar{q}$ central system or to a quark in the proton is purely perturbative (given at the hard scale $\mu_F \sim M_{q\bar{q}\perp}$) and enters to the hard subprocess amplitude.

In the forward limit the following factorization is assumed

$$f_g^{\text{off}}(x', x_{1,2}, q_{1/2\perp}^2, q_{0\perp}^2, \mu_F^2; t) = f_g^{\text{off}}(x', x_{1,2}, q_{1/2\perp}^2, q_{0\perp}^2, \mu_F^2) \exp(bt/2), \quad (3.21)$$

with the slope parameter $b \simeq 4 \text{ GeV}^{-2}$ [26]. In the $x' \ll x_{1,2}$ limit the off-diagonal UGDFs can be written as [27, 28]

$$f_g^{\text{off}}(x', x_{1,2}, q_{1/2\perp}^2, q_{0\perp}^2, \mu_F^2) \simeq R_g(x') \cdot f_g(x_{1,2}, q_{1/2\perp}^2, \mu_F^2), \quad (3.22)$$

where the skewedness parameter $R_g \simeq 1.2 - 1.3$ is roughly constant at LHC energies, which accounts for the single $\log Q^2$ skewed effect [29] and gives only a small contribution to an overall normalization uncertainty.

Another more symmetrical prescription for skewed UGDFs was introduced in Refs. [30, 31]. It is inspired by the positivity constraints for the collinear Generalized Parton Distributions [32], and can be considered as a saturation of the Cauchy-Schwarz inequality for the density matrix [33]. It allows us to incorporate the actual dependence of the off-diagonal UGDFs on longitudinal momentum fraction of the soft screening gluon and its transverse momentum in explicitly symmetric way:

$$f_{1/2g}^{\text{off}} \simeq \sqrt{f_g(x_{1,2}, q_{1/2\perp}^2, \mu_F^2) \cdot f_g(x', q_{0\perp}^2, \mu_{\text{soft}}^2)}, \quad x' \sim \frac{q_{0\perp}}{\sqrt{s}}. \quad (3.23)$$

As we see it explicitly depends on $x' \sim q_{0\perp}^2/s$. It works well in the description of the recent CDF data on the central exclusive charmonia production [31, 34] and the precise HERA data on the diffractive structure function [35]. Model (3.23) implies the factorization of the generalized UGDF into the hard part depending on a hard scale μ_F and $x_{1,2}$ describing the hard gluon coupling to the proton, and the soft part defined at some soft scale μ_{soft} and small $x' \ll x_{1,2}$. Together with the factorization in transverse momentum space, model (3.23) provides the QCD factorization of the diffractive amplitude in the full momentum space.

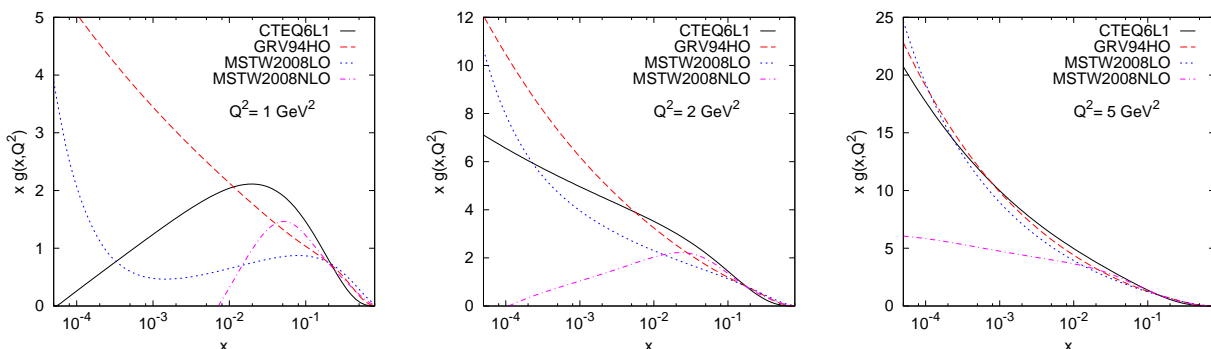


FIG. 6: Gluon densities as a function of longitudinal momentum fraction x at the scales $Q^2 = 1, 2$ and 5 GeV^2 given by the global parameterizations CTEQ6L1 [44], GRV94HO [42], MSTW2008LO and NLO [45].

In the considered kinematics the diagonal unintegrated densities can be written in terms of the conventional (integrated) densities $xg(x, q_{\perp}^2)$ as [28]

$$f_g(x, q_{\perp}^2, \mu^2) = \frac{\partial}{\partial \ln q_{\perp}^2} [xg(x, q_{\perp}^2) \sqrt{T_g(q_{\perp}^2, \mu^2)}], \quad (3.24)$$

where T_g is the Sudakov form factor which suppresses real emissions from the active gluon during the evolution, so that the rapidity gaps survive. It is given by

$$T_g(q_\perp^2, \mu^2) = \exp\left(-\int_{q_\perp^2}^{\mu^2} \frac{d\mathbf{k}_\perp^2}{\mathbf{k}_\perp^2} \frac{\alpha_s(k_\perp^2)}{2\pi} \int_0^{1-\Delta} \left[zP_{gg}(z) + \sum_q P_{qg}(z) \right] dz\right), \quad (3.25)$$

where the upper limit is taken to be

$$\Delta = \frac{k_\perp}{k_\perp + aM_{q\bar{q}}}. \quad (3.26)$$

The KMR group used $a = 0.62$ [36]. It was argued recently that $a = 1$ should be used instead [37], so in numerical calculations below we adopt the last choice (for these two choices the final results for the Higgs CEP cross section differ by about a factor of 2, which is not negligible). In addition, following Ref. [37] we use the factorization scale $\mu_F = M_{q\bar{q}}$ as compared to the KKMR choice $\mu_F^{\text{KMR}} = M_{q\bar{q}}/2$. We will discuss the sensitivity to the factorization scale choice below when presenting numerical results.

In general, employing diagonal UGDF in the form (3.24) we encounter a problem of poorly known gluon PDFs at rather low $x_{1,2}$ and especially small gluon virtualities q_\perp^2 . For an illustration of the corresponding uncertainties, in Fig. 6 we show several gluon PDFs as functions of fraction x at evolution scale $\sim q_\perp^2$ fixed at values 1, 2 and 5 GeV² characteristic for the exclusive production of Higgs boson. We see that at $x \lesssim 10^{-3}$ the PDF uncertainties may strongly affect predictions for not sufficiently large gluon transverse momenta. In this sense, the precise data on the diffractive and central exclusive production could be used for making constraints on the PDF parameterizations [35].

Testing other models of UGDFs, different from Eq. (3.24), may be important for estimation of an overall theoretical uncertainty of our predictions and their stability.

IV. ELECTROMAGNETIC $\gamma^*\gamma^*$ -FUSION PROCESS

It is instructive to estimate the QED contribution to the central exclusive $b\bar{b}$ production illustrated in Fig. 7.

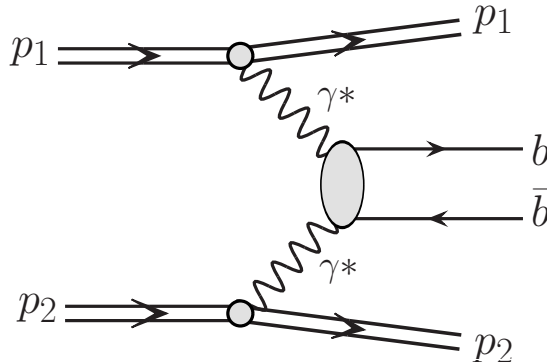


FIG. 7: The QED $\gamma^*\gamma^*$ fusion mechanism of the exclusive $q\bar{q}$ production.

In the forward limit of small momentum transfers $t_{1,2}$ ($|t_{1,2}| \ll 4m_N^2$) the matrix element for $pp \rightarrow pp q\bar{q}$ reaction via $\gamma^*\gamma^*$ -fusion can be written as [30]

$$\mathcal{M}^{\gamma^*\gamma^*} \approx eF_1(t_1) \frac{(p_1 + p'_1)^\nu}{t_1} V_{\mu\nu}^{\gamma^*\gamma^*}(q_1, q_2) \frac{(p_2 + p'_2)^\mu}{t_2} eF_1(t_2), \quad (4.1)$$

where $F_1(t_1)$ and $F_1(t_2)$ are Dirac proton electromagnetic form factors, and the $\gamma^*\gamma^* \rightarrow q\bar{q}$ vertex [31] has analogous form as (3.4), i.e.

$$V_{\lambda_q\lambda_{\bar{q}},\mu\nu}^{\gamma^*\gamma^*} = (e_q e)^2 \bar{u}_{\lambda_q}(k_1) \left(\gamma^\nu \frac{\hat{q}_1 - \hat{k}_1 - m_q}{(q_1 - k_1)^2 - m_q^2} \gamma^\mu - \gamma^\mu \frac{\hat{q}_1 - \hat{k}_2 + m_q}{(q_1 - k_2)^2 - m_q^2} \gamma^\nu \right) v_{\lambda_{\bar{q}}}(k_2). \quad (4.2)$$

Momentum conservation dictates us the following decompositions of the photon momenta into the longitudinal and transverse parts w.r.t. c.m.s. direction [31]:

$$q_1 = x_1 p_1 + \frac{t_1}{s} p_2 + q_{1\perp}, \quad q_2 = x_2 p_2 + \frac{t_2}{s} p_1 + q_{2\perp}, \quad q_{1/2\perp}^2 \simeq t_{1,2}(1 - x_{1,2}), \quad (4.3)$$

where $t_{1,2} \equiv q_{1,2}^2$. Due to gauge invariance we have (similarly to (3.10))

$$V^{\gamma^*\gamma^*}(q_1, q_2) = (p_1 + p'_1)^\nu V_{\mu\nu}^{\gamma^*\gamma^*}(q_1, q_2) (p_2 + p'_2)^\mu = 4p_1^\nu p_2^\mu V_{\mu\nu}(q_1, q_2). \quad (4.4)$$

so the matrix element squared $|V^{\gamma^*\gamma^*}|^2$ is proportional to the gluonic one found in Eq. (3.13). The photon virtualities in the relevant limit disappear $t_{1,2} \rightarrow 0$, so $q_\perp \rightarrow 0$ leading to vanishing of the $\gamma^*\gamma^* \rightarrow q\bar{q}$ amplitude in the high- k_\perp limit and massless quarks (see Eq. (3.13)). Thus, to estimate $\gamma^*\gamma^*$ contribution to exclusive production of quark jets we have to take into account subleading corrections in the m_q/k_\perp -expansion. This means that the electromagnetic mechanism may give some contribution for moderate and large quark masses, which will be evaluated numerically in the Results section.

V. OFF-SHELL EFFECTS IN CENTRAL EXCLUSIVE HIGGS PRODUCTION

As one can see from Eq. (3.10), the subprocess vertex $V_{\lambda_q\lambda_{\bar{q}}}$ of $g^*g^* \rightarrow b\bar{b}$ is proportional to gluon transverse momenta squared due to projection $\sim q_{1\perp}^\mu q_{2\perp}^\nu$. When considering the irreducible $b\bar{b}$ background for Higgs boson production in the amplitude $V_{\lambda_q\lambda_{\bar{q}}}^{\mu\nu}$ we can neglect, in principle, the gluon virtualities in comparison with quark transverse momenta k_\perp and b -quark mass m_q as it was done in e.g. Ref. [5].

However, as demanded by k_\perp -factorization framework, it may be instructive to analyze in which region of the phase space the gluon off-shell effects may play a significant role (if any), and whether it is possible to see such effects in experiment. A complete calculation of the off-shell effects in inclusive Higgs boson production was performed in Ref. [38] (for the Higgs boson production in k_\perp -factorisation, see also Ref. [39]). It was shown there that the off-shell effects can significantly affect the distribution of Higgs boson cross section in azimuthal angle between fusing gluons ϕ in a very close vicinity of $\phi = \pi/2$. The calculations of the central exclusive Higgs production rates in the on-shell gluon approximation are well-known [4]. Let us now investigate off-shell effects in Higgs CEP.

A. Off-shell effects in the hard vertex $g^*g^* \rightarrow H$

Tensor decomposition of the hard subprocess amplitude $g^*g^* \rightarrow H$ can be written in the following general form [38]

$$T_{\mu\nu}^{ab}(q_1, q_2) = i\delta^{ab}\frac{\alpha_s}{2\pi}\frac{1}{v}\left([(q_1q_2)g_{\mu\nu} - q_{1,\nu}q_{2,\mu}]G_1 + \left[q_{1,\mu}q_{2,\nu} - \frac{q_1^2}{(q_1q_2)}q_{2,\mu}q_{2,\nu} - \frac{q_2^2}{(q_1q_2)}q_{1,\mu}q_{1,\nu} + \frac{q_1^2q_2^2}{(q_1q_2)^2}q_{1,\nu}q_{2,\mu} \right] G_2 \right), \quad (5.1)$$

where α_s is the strong coupling constant, $v = (G_F\sqrt{2})^{-1/2}$ is the electroweak parameter of the Standard Model, a, b are the colour indices of two virtual gluons with momenta q_1, q_2 .

Let us introduce the dimensionless parameters

$$\chi = \frac{M_H^2}{4m_f^2} > 0, \quad \chi_1 = \frac{q_1^2}{4m_f^2} < 0, \quad \chi_2 = \frac{q_2^2}{4m_f^2} < 0,$$

so the heavy quark limit corresponds to $\chi, \chi_1, \chi_2 \rightarrow 0$. In the case of heavy Higgs production we have $M_H^2 \gg |\mathbf{q}_{1\perp}|^2, |\mathbf{q}_{2\perp}|^2$, so in the expansion of the form factors we have to take into account powers of χ higher than powers of gluon virtualities χ_1, χ_2 [38]

$$G_1(\chi, \chi_1, \chi_2) = \frac{2}{3} \left[1 + \frac{7}{30}\chi + \frac{2}{21}\chi^2 + \frac{11}{30}(\chi_1 + \chi_2) + \dots \right],$$

$$G_2(\chi, \chi_1, \chi_2) = -\frac{1}{45}(\chi - \chi_1 - \chi_2) - \frac{4}{315}\chi^2 + \dots \quad (5.2)$$

These expansions will be sufficient for our present calculations.

Let us turn now to the discussion of the exclusive diffractive Higgs production within the KKMR double diffractive mechanism [4]. The hard subprocess vertex entering the diffractive amplitude (3.1) $V \equiv V(q_{1\perp}^2, q_{2\perp}^2, P_\perp^2)$ with explicit taking into account gluon virtualities reads

$$V_{g^*g^* \rightarrow H}^{ab}(q_{1\perp}^2, q_{2\perp}^2, P_\perp^2) = n_\mu^+ n_\nu^- T_{\mu\nu}^{ab}(q_1, q_2) = \frac{4}{s} \frac{q_{1\perp}^\mu}{x_1} \frac{q_{2\perp}^\nu}{x_2} T_{\mu\nu}^{ab}(q_1, q_2), \quad q_1^\mu T_{\mu\nu}^{ab} = q_2^\nu T_{\mu\nu}^{ab} = 0, \quad (5.3)$$

where the amplitude of the gluon fusion $T_{\mu\nu}^{ab}(q_1, q_2)$ is defined in Eq. (5.1). Contracting indices and introducing the transverse Higgs mass,

$$sx_1x_2 = M_H^2 - P_\perp^2 \equiv M_{H\perp}^2, \quad P_\perp^2 = -|\mathbf{P}_\perp|^2 = -(\mathbf{q}_{1\perp}^2 + \mathbf{q}_{2\perp}^2 + 2|\mathbf{q}_{1\perp}||\mathbf{q}_{2\perp}|\cos\phi), \quad (5.4)$$

we get in terms of form factors (5.2)

$$V_{g^*g^* \rightarrow H}^{ab} = -i\delta^{ab}\frac{\alpha_s}{\pi}\frac{|\mathbf{q}_{1\perp}||\mathbf{q}_{2\perp}|}{v}\left[\cos\phi G_1 - \frac{2M_{H\perp}^2|\mathbf{q}_{1\perp}||\mathbf{q}_{2\perp}|}{(M_H^2 + \mathbf{q}_{1\perp}^2 + \mathbf{q}_{2\perp}^2)^2} G_2 \right]. \quad (5.5)$$

In the limit of real gluons for not extremely heavy Higgs we have asymptotically

$$V_{gg \rightarrow H}^{ab} \simeq -i\delta^{ab}\frac{\alpha_s}{\pi}\frac{1}{v}(\mathbf{q}_{1\perp}\mathbf{q}_{2\perp}) \cdot \frac{2}{3}, \quad (\mathbf{q}_{1\perp}\mathbf{q}_{2\perp}) = |\mathbf{q}_{1\perp}||\mathbf{q}_{2\perp}|\cos\phi. \quad (5.6)$$

Substituting this into the amplitude (3.1), we get after summation over colour indices

$$\mathcal{M}_{excl}^{\text{on-shell}} = \frac{\pi\alpha_s}{v} \cdot \frac{s}{3} \int d^2\mathbf{q}_{0\perp} \frac{(\mathbf{q}_{1\perp}\mathbf{q}_{2\perp})}{\mathbf{q}_{0\perp}^2 \mathbf{q}_{1\perp}^2 \mathbf{q}_{2\perp}^2} f_{g,1}^{\text{off}}(x_1, x', q_{0\perp}^2, q_{1\perp}^2, t) f_{g,2}^{\text{off}}(x_2, x', q_{0\perp}^2, q_{2\perp}^2, t_2),$$

Next-to-leading order contribution in the cross section of the hard subprocess $\hat{\sigma}(gg \rightarrow H)$ can be accounted for by a factor $K_{NLO} \simeq 1.5$ assuming that the NLO corrections factor K_{NLO} in the $g^*g^* \rightarrow H$ vertex is the same as in the $H \rightarrow gg$ width provided that $|V_{gg \rightarrow H}|^2 \sim \Gamma(H \rightarrow gg)$ [40]. As for the irreducible Higgs background, the one-loop corrections to $gg \rightarrow b\bar{b}$ were calculated in Ref. [7]. For simplicity, in the current analysis we do not take into account the NLO effects and concentrate only on the leading order contributions in the hard subprocess part.

At high energies the cross section for the exclusive Higgs boson production can be expressed as:

$$d\sigma_{pp \rightarrow pHp} = \frac{1}{2s} |\mathcal{M}|^2 \cdot d^3PS, \quad d^3PS = \frac{1}{28\pi^4 s} dt_1 dt_2 dy_H d\Phi.$$

B. $b\bar{b}$ signal of the Higgs decay

In order to estimate the observable signal from the central exclusive production of Higgs in the $b\bar{b}$ decay channel, one can multiply the matrix element squared $|\mathcal{M}_{excl}|^2$ by the relativistic Breit-Wigner distribution over the invariant mass $\mu \equiv M_{b\bar{b}}$ of $b\bar{b}$ pair with a proper normalization

$$\rho_{b\bar{b}}(\mu) = \frac{1}{\pi} \frac{\mu \Gamma_H^{b\bar{b}}(\mu)}{[\mu^2 - M_H^2]^2 + [\mu \Gamma_H^{tot}(\mu)]^2}, \quad (5.7)$$

and then integrate it out over the 4-particle $p(b\bar{b})p$ invariant phase space. In Eq. (5.7) the total Higgs decay width into fermions and gluons is (see e.g. Ref. [41])

$$\Gamma_H^{tot}(M_H) = \Gamma_H^{f\bar{f}}(M_H) + \Gamma_H^{gg}(M_H), \quad (5.8)$$

$$\Gamma_H^{f\bar{f}}(M_H) = \frac{g^2 M_H}{32 \pi M_W^2} \left\{ 3 [m_b^2(M_H) + m_c^2(M_H)] \left[1 + 5.67 \frac{\alpha_s(M_H)}{\pi} + 42.74 \left(\frac{\alpha_s(M_H)}{\pi} \right)^2 \right] + m_\tau^2 \right\},$$

$$\Gamma_H^{gg}(M_H) = \frac{g^2 M_H^3}{288 \pi M_W^2} \frac{\alpha_s^2(M_H)}{\pi^2} \left\{ 1 + 17.91667 \frac{\alpha_s(M_H)}{\pi} \right\}$$

and the partial Higgs decay width into $b\bar{b}$ channel is given by

$$\Gamma_H^{b\bar{b}}(M_H) = \frac{3g^2 M_H}{32 \pi M_W^2} m_b^2(M_H) \left[1 + 5.67 \frac{\alpha_s(M_H)}{\pi} + 42.74 \left(\frac{\alpha_s(M_H)}{\pi} \right)^2 \right]. \quad (5.9)$$

Above, $g^2 = 0.42502$ is the electromagnetic coupling constant, and $m_{c,b}(\mu)$ and $\alpha_s(\mu)$ are the running quark masses and the QCD coupling constant, respectively. For example, at $M_H = 100$ GeV, they are $m_c(M_H) = 0.542$ GeV, $m_b(M_H) = 2.676$ GeV and $\alpha_s(M_H) = 0.12121$. Substituting these values into Eq. (5.8) we get the total decay width $\Gamma_H^{tot}(M_H) = 2.268$ MeV which coincides with the number given in Ref. [41].

VI. NUMERICAL RESULTS

In this section we will present differential distributions for central exclusive heavy quark dijets and Higgs production. We show also distributions of b and \bar{b} quarks from the decay of the Higgs boson. We start from the presentation of the results for heavy quark ($c\bar{c}$ and $b\bar{b}$) production. Very important part of the analysis below concerns the $b\bar{b}$ background below the $b\bar{b}$ Higgs signal.

A. Differential distributions for exclusive $c\bar{c}$ and $b\bar{b}$ pair production

We start our presentation from the distribution in heavy quark invariant mass. In Fig. 8 we show distributions for $c\bar{c}$ (left panel) and $b\bar{b}$ (right panel) for different gluon collinear distributions used to generate UGDFs, for quark rapidities $y_q, y_{\bar{q}} \in (-2.5, 2.5)$. We show distributions for QCD diffractive mechanism as well as for the QED $\gamma^*\gamma^*$ fusion. Only at small invariant masses is the distribution for $c\bar{c}$ higher than that for $b\bar{b}$. The position of the peak of the distributions depends on the quark mass and is placed slightly above $2m_q$, both for diffractive and QED components. Relative contribution of QED mechanism grows with increasing invariant $q\bar{q}$ mass, and starts to dominate at $M_{q\bar{q}} \gtrsim 60$ GeV for $c\bar{c}$ and $M_{q\bar{q}} \gtrsim 120$ GeV for $b\bar{b}$.

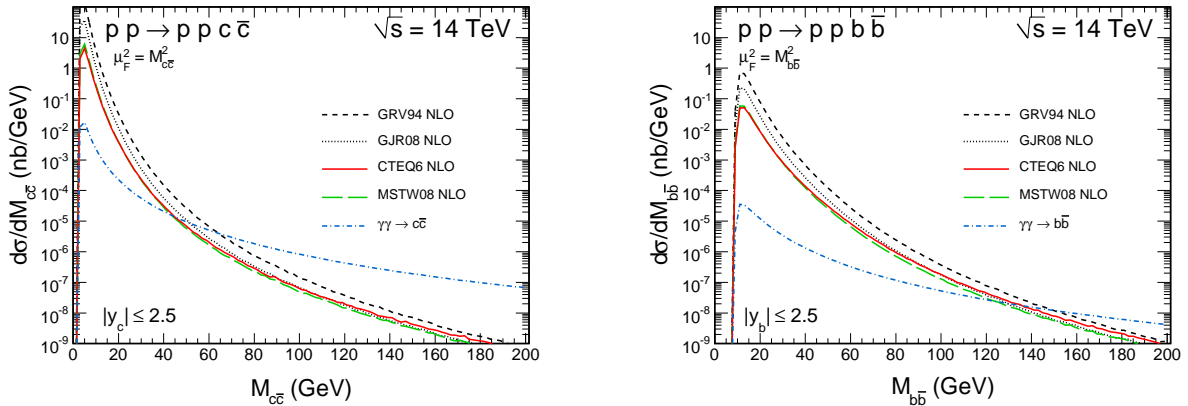


FIG. 8: Invariant mass $M_{q\bar{q}}$ distributions for the central exclusive production of $c\bar{c}$ (left panel) and $b\bar{b}$ (right panel) dijets at LHC. Results for diffractive component are shown for a few GDFs from the literature: GRV94 NLO [42] (dashed line), GJR08 NLO [43] (dotted line), CTEQ6 NLO [44] (solid line) and MSTW2008 NLO [45] (long-dashed line). QED $\gamma^*\gamma^*$ fusion contribution is illustrated by the dash-dotted line. Experimental cuts on quark (antiquark) rapidities $|y_q| \leq 2.5$ are included. The distribution is then integrated over whole invariant $q\bar{q}$ mass range $2m_q < M_{q\bar{q}} < 200$ GeV in order to get the total cross section.

There is a strong sensitivity of the invariant mass distribution on the gluon PDFs. In particular, the difference of the results for the GRV94 NLO [42] and CTEQ6 NLO [44] is up to an order of magnitude in the peak. The QED contribution is found to be smaller than that for the diffractive mechanism but it is very important as background to the exclusive Higgs boson production. In this calculation only the Dirac F_1 proton electromagnetic form

factor is included. The contribution of the Pauli F_2 proton electromagnetic form factor is expected to be negligible.

For the bulk of the $c\bar{c}$ or $b\bar{b}$ production $M_{q\bar{q}}$ is only slightly larger than the quark masses. Nevertheless what matters is that $M_{q\bar{q}}$ is in the perturbative region. We can go down with transverse momenta of gluons as low as $q_{\perp}^2 \sim 0.4 \text{ GeV}^2$. Of course it is not easy to predict what happens in the nonperturbative region. In the present paper we concentrate on large quark-antiquark invariant masses where the issue is not so important.

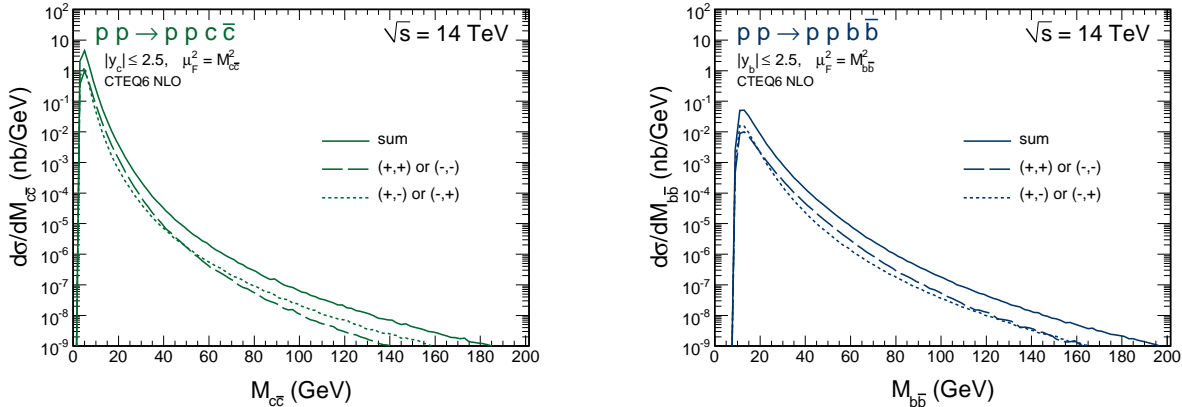


FIG. 9: Invariant mass distributions of centrally produced $c\bar{c}$ pair (left panel) and $b\bar{b}$ pair (right panel) for different (anti)quark helicities $\lambda_q\lambda_{\bar{q}} = ++, -+$ and for the sum over all quark helicity states. CTEQ6 PDF was used here. Kinematical constraints are the same as in Fig. 8.

There was recently [7] a discussion about the contribution of different helicity states to the cross section. In Fig. 9 we show individual contributions for different quark helicities $\lambda_q\lambda_{\bar{q}} = ++$ and $-+$ (other helicity contributions are the same due to symmetry as discussed above). The contributions of the same and opposite quark helicities are rather similar in the broad range of the quark-antiquark pair invariant masses. In particular, they are almost identical in the region of typical light Higgs mass.

The cross section for the diquark production strongly depends on the quark masses thus underlying the importance on the finite b -quark masses for the CEP Higgs background evaluation. This is encoded in the matrix elements discussed in the theory section. In Fig. 10 we have collected the results for the total (left panel) and differential in quark-antiquark invariant mass (right panel) cross sections. The total cross section slightly grows with the quark mass. The growth is, however, slower than in Ref. [7] where the matrix element is proportional to the quark mass. Taken a typical misidentification probability and the fact that light quark cross sections are smaller than that for $b\bar{b}$ in the Higgs region, the latter is in practice the only troublesome background. Our result is very interesting in the context of diffractive dijet production. Recently the CDF collaboration has measured the corresponding cross section at the Tevatron [3]. The quark jets are usually neglected and only gluonic jets are included in theoretical calculations (for the gluonic jets analysis, see e.g. Ref. [9]). The quark jets contribution to the CDF data will be discussed elsewhere [25].

Let us come now to the rapidity distributions. The distribution in quark (antiquark) rapidity in the detector interval, integrated over whole invariant mass range of $M_{q\bar{q}} \in (2m_q, 200) \text{ GeV}$, is shown in Fig. 11. The distribution for charm quarks is flatter than that for the bottom quarks. For comparison, we also show the corresponding distributions

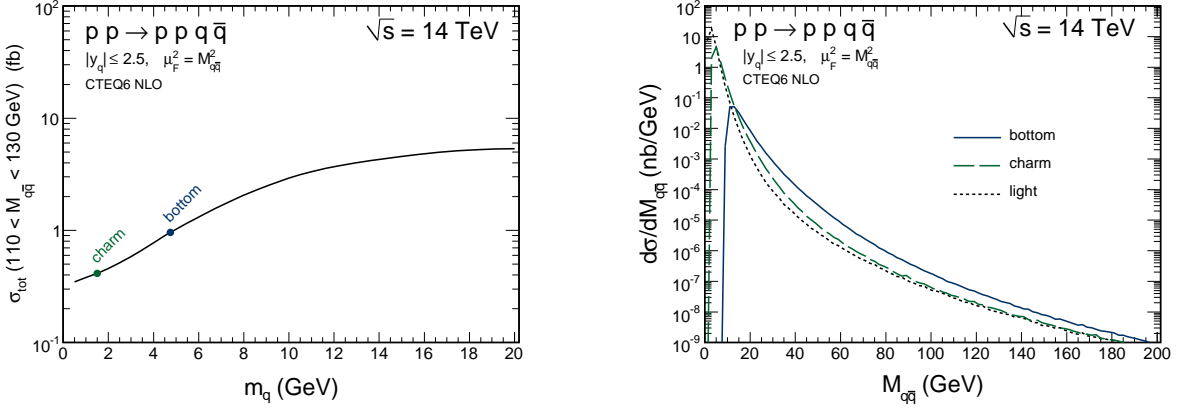


FIG. 10: The EDD $q\bar{q}$ cross section in the vicinity of the Higgs mass as a function of quark mass(left panel) and invariant mass distributions of the EDD $q\bar{q}$ production for different quark masses. Kinematical constraints are the same as in Fig. 8.

for different combinations of quark helicities $\lambda_q \lambda_{\bar{q}} = ++$ and $-+$. As for the quark-antiquark invariant mass distributions, the same and opposite helicity contributions are similar. The rapidity distributions shown are dominated by the low quark-antiquark invariant masses.

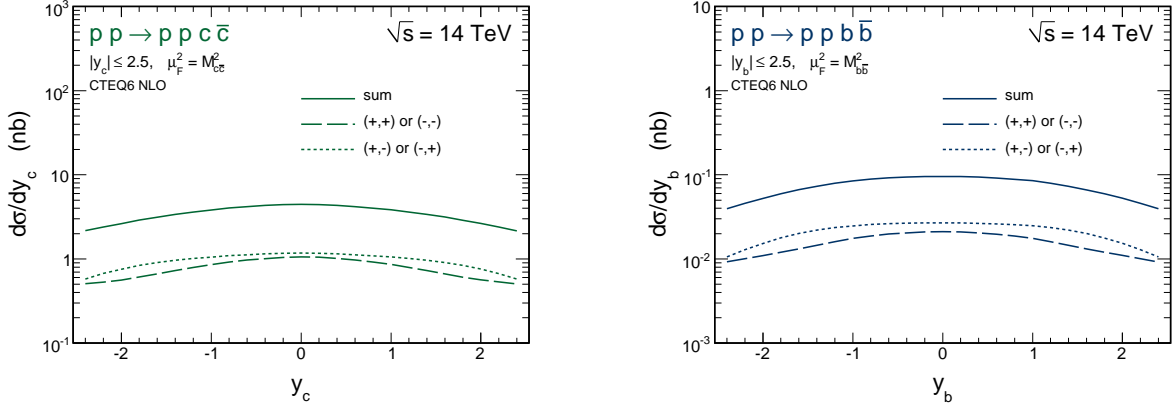


FIG. 11: Differential distributions in quark (antiquark) rapidity of EDD c or \bar{c} (left panel) and b or \bar{b} (right panel). Kinematical constraints are the same as in Fig. 8.

In Fig. 12 we show distribution in the rapidity of the $q\bar{q}$ pair. Here the distribution of the opposite quark helicity is much flatter than the distribution of the same quark helicity. This distribution may, however, be slightly biased by the limitation of the individual rapidities of the quark and antiquark.

Let us come now to transverse momentum distributions. In Fig. 13 we show distribution in quark (antiquark) transverse momenta. These distributions are extended to large transverse momenta with the peak at about 2 GeV for c/\bar{c} and 3 GeV for b/\bar{b} . This is fully perturbative effect and is encoded in the $g^*g^* \rightarrow q\bar{q}$ matrix elements discussed in Sections III and IV. One can clearly see the dominance of the opposite sign helicities contribution at large transverse momenta. For comparison, we show also distribution in proton transverse momenta (dashed line). In contrast to quarks (antiquarks) p_{\perp} -distributions, they are order

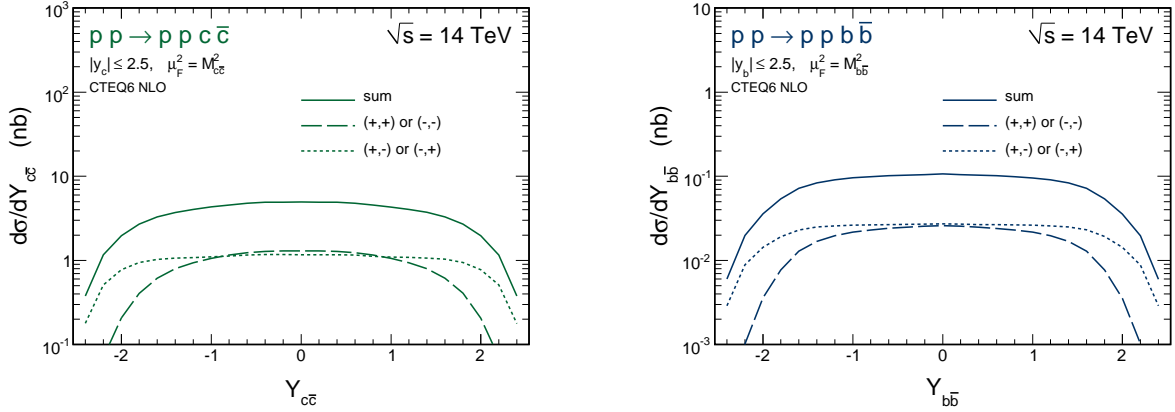


FIG. 12: Differential distributions in rapidity of the $c\bar{c}$ pair $Y_{c\bar{c}}$ (left panel) and $b\bar{b}$ pair $Y_{b\bar{b}}$ (right panel). Kinematical constraints are the same as in Fig. 8.

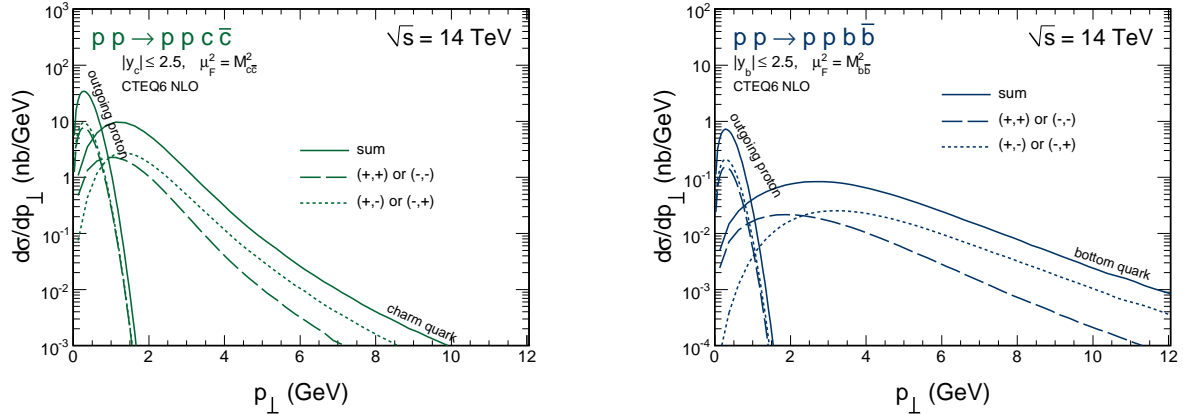


FIG. 13: Differential distributions in transverse momenta of quark (antiquark) (solid line) and outgoing protons (dashed line) of EDD $c\bar{c}$ (left panel) and $b\bar{b}$ (right panel) cross section. Kinematical constraints are the same as in Fig. 8.

of magnitude narrower and concentrated below 1 GeV with maximum at about 0.3 GeV. These distributions are controlled by a nonperturbative proton form factor and are thus sensitive to internal structure of the proton.

The distribution in the total transverse momentum of the $q\bar{q}$ pair $|\mathbf{p}_{q\bar{q}\perp}|$ (by definition $\mathbf{p}_{q\bar{q}\perp} = \mathbf{p}_{q\perp} + \mathbf{p}_{\bar{q}\perp}$) is shown in Fig. 14. It is much narrower than that for the individual quark (antiquark). The maximum of the cross section is at about 0.5 GeV. Similarly as the distributions in the proton transverse momentum is fully nonperturbative and related to the slope of the nucleon form factors.

Finally, let us turn to azimuthal angle correlations. We will consider correlations between outgoing quark jets, as well as between outgoing protons.

In Fig. 15 we show correlations between outgoing jets without extra cuts on jets transverse momenta. Even without such cuts the quark and antiquark are strongly correlated with a preference for the back-to-back configuration. The deviation from the back-to-back configuration is caused by the transverse momenta of gluons in the ladder. If there were no

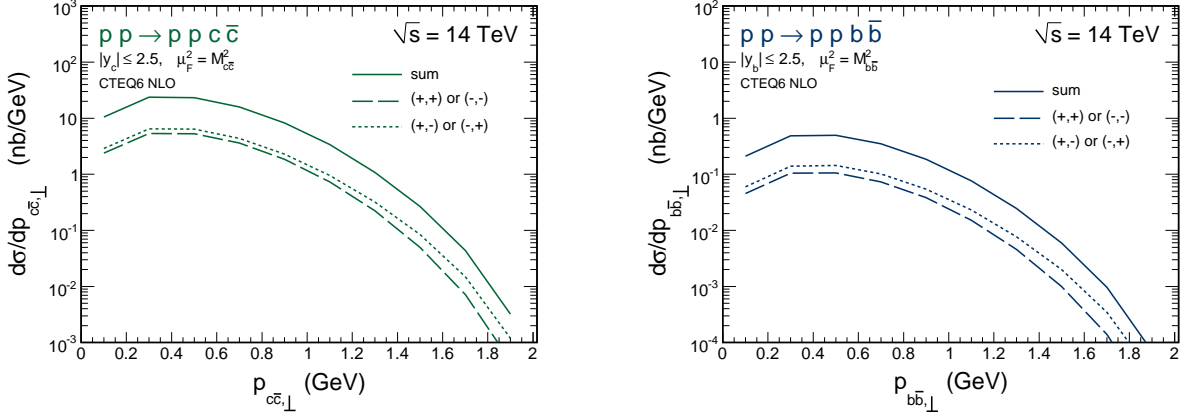


FIG. 14: Differential distributions in transverse momenta of quark-antiquark pair $|\mathbf{p}_{q\bar{q}\perp}|$. Kinematical constraints are the same as in Fig. 8.

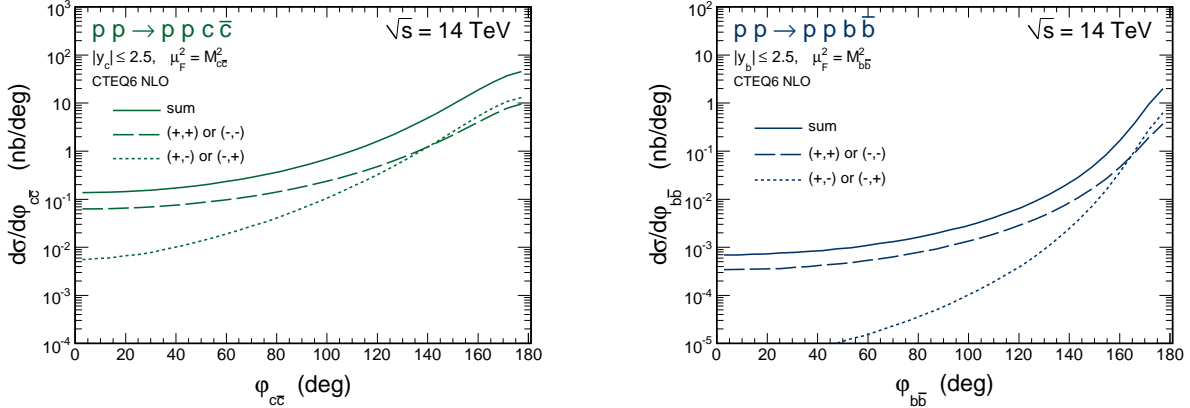


FIG. 15: Differential distributions in azimuthal angle between c, \bar{c} jets (left panel) and b, \bar{b} jets (right panel). Kinematical constraints are the same as in Fig. 8.

transverse momenta of initial gluons, final jets would be back-to-back which follows from the kinematics of the process. There is a stronger helicity correlation for the opposite quark helicities than that for the same quark helicities. The correlation would even increase when imposing extra cuts on quark (antiquark) transverse momenta.

In Fig. 16 we show correlations between outgoing protons. In contrast to quarks (antiquarks) protons are almost decorrelated. This can be understood post factum taken complicated gluonic ladders spanned between protons and quarks. The soft rescattering effects could further modify the distribution (see e.g. [26, 46]).

Finally, we would like to show a two-dimensional distribution which is very useful when discussing background to the exclusive Higgs boson production in the $b\bar{b}$ channel. In Fig. 17 we show the distribution in $M_{b\bar{b}}$ and transverse momentum of the quark ($p_{b\perp}$) for EDD (left panel) and QED (right panel) mechanisms. One can clearly see that a fixed mass (e.g. mass of the Higgs) can be obtained both for high and low transverse momenta of the quark jets. The latter case can be realized when the quark rapidities are large. For EDD contribution one can remove such cases by imposing cuts on jet transverse momenta. One

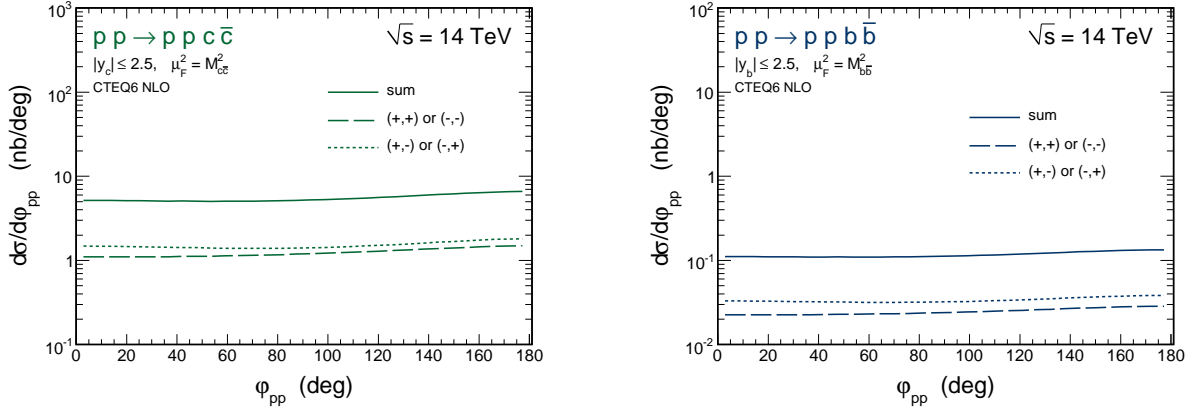


FIG. 16: Differential distributions in angle between outgoing protons corresponding to $c\bar{c}$ EDD (left panel) and $b\bar{b}$ EDD (right panel). Kinematical constraints are the same as in Fig. 8.

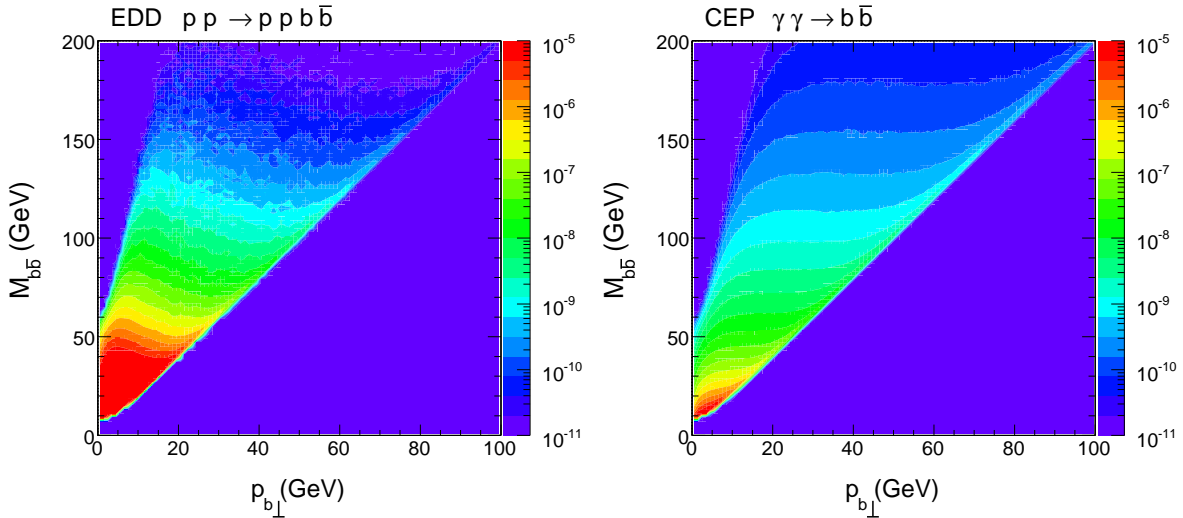


FIG. 17: Two-dimensional distribution in invariant $b\bar{b}$ mass $M_{b\bar{b}}$ and (anti)quark transverse momentum $p_{b\perp}$. Kinematical constraints are the same as in Fig. 8.

could equivalently limit quark (antiquark) rapidities. We will return to these correlations when discussing the Higgs background.

B. Central exclusive production of Higgs boson

Due to a very large hard scale of the process $\sim M_H$, the influence of typically small gluon virtualities in the amplitude of hard subprocess amplitude (5.5), as well as the role of form factor G_2 , in the exclusive diffractive Higgs production turned out to be quite small, in analogy to the inclusive case [38].

The integrated cross section of diffractive Higgs production at the LHC energy $\sqrt{s} = 14$ TeV, taking into account the “effective” gap survival factor $\langle S^2 \rangle \simeq 0.03$ [4], calculated for typical Higgs mass $M_H = 120$ GeV is $\sigma_{tot} \lesssim 1$ fb. Our result is smaller than that found by the Durham group. As discussed above this is mostly due to different choice of the scale

of the Sudakov form factor. The result of Cudell, Hernandez, Ivanov and Dechambre [9] is closer to our result but still slightly bigger. This is probably due to different unintegrated gluon distribution. In particular, the Ivanov-Nikolaev UGDF used in their analysis includes also a nonperturbative piece fitted to the data.

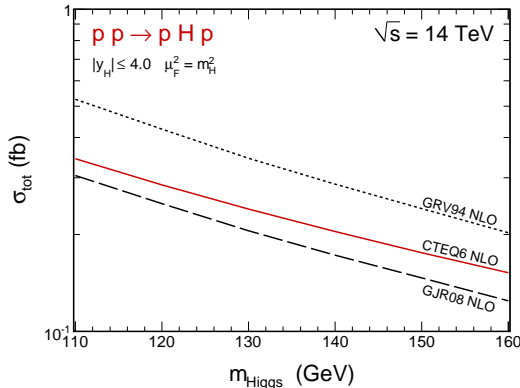


FIG. 18: Total cross section for exclusive Higgs production for different gluon PDFs from the literature. The calculation was done including off-shell effects.

In Fig. 18 we show the total cross section for exclusive production of Higgs boson as a function of the Higgs mass for different gluon distributions for $\sqrt{s} = 14$ TeV. The difference between different gluon PDFs comes mainly from a different lower cut-off parameter for gluon transverse momenta in different gluon distributions. This is necessary and is dictated by the construction of different UGDFs. In particular, different groups choose different initial scale for QCD evolution and going below it often leads to unphysical solutions (negative glue for instance). This forces one to put lower cut-off at the value of the initial scale. The cross section for exclusive Higgs production obtained here is rather small².

We have made the calculation of the cross section in the limit of real gluons in the hard part (5.6) (σ_H^{on}), as well as with an account of gluon virtualities (5.5) (σ_H^{off}). Contribution of non-zeroth q_1^2, q_2^2 in form factors $G_{1,2}$ turns out to be negligibly small; difference between σ_H^{on} and σ_H^{off} is formed mainly by the second form factor G_2 , and gives about 6 %, so it is much smaller than other theoretical uncertainties of the approach. The overall uncertainty of 0^+ Higgs CEP cross section was estimated in Ref. [4] to be up to a factor of 2.5.

In Fig. 19 we show a two-dimensional distribution of the Higgs in its rapidity and transverse momentum. The Higgs production is concentrated around rapidity $y = 0$ and the cross section quickly drops with Higgs transverse momentum. In Fig. 20 we show respective projections on rapidity (left panel) and transverse momentum (right panel). The maximum of the transverse momentum dependence occurs at about 0.4 GeV. The distribution reflects a convolution of the nucleon form factors, i.e. is of purely nonperturbative nature.

Finally, we focus on angular correlations (see Fig. 21). In the figure we show distribution in azimuthal angle between outgoing protons. As for the exclusive production of heavy quarks there is a very small correlation between outgoing protons.

Note that the distribution in relative azimuthal angle between protons ϕ_{pp} strongly differs from the distributions in azimuthal angle $\phi_{\mathbf{q}_1, \mathbf{q}_2}$ between interacting gluons $\sim \cos^2 \phi_{\mathbf{q}_1, \mathbf{q}_2}$ due

² Similarly small cross sections have been obtained very recently [15] when this paper was already finished.

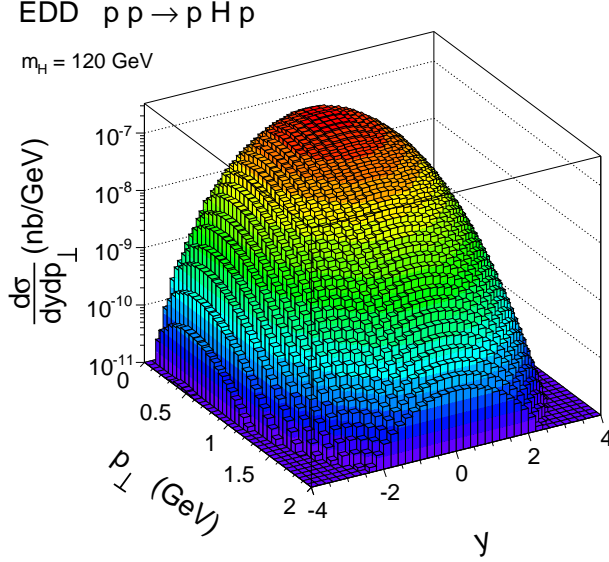


FIG. 19: A two-dimensional distribution in the Higgs rapidity (y) and Higgs transverse momentum (p_{\perp}) for CTEQ6 gluon PDF.

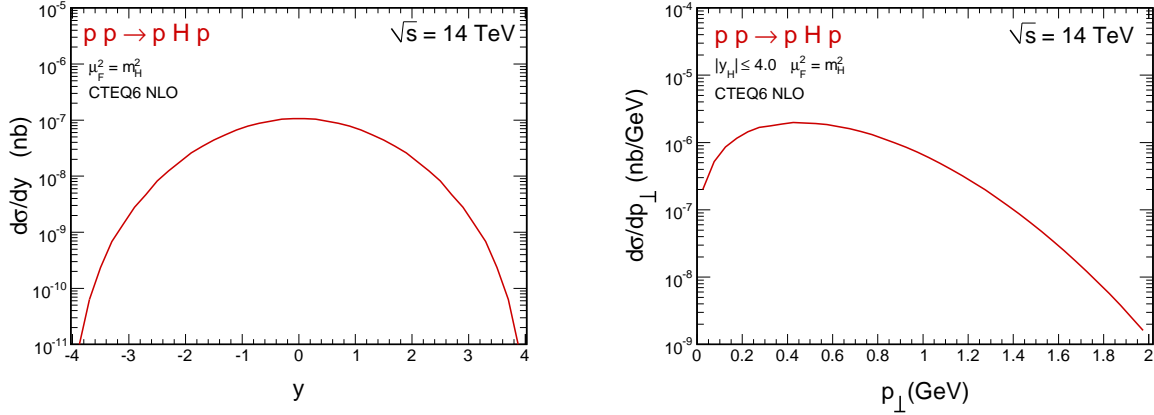


FIG. 20: Rapidity (left) and transverse momentum (right) distributions of the Higgs boson. CTEQ6 PDF was used in this calculation.

to the convolution with momentum transfer $q_{0\perp}$ of the screening gluon. Only in the case when Higgs boson production is governed by e.g. pomeron-pomeron (or $\gamma^*\gamma^*$) fusion, the angle between pomerons (photons) coincides with the angle between outgoing protons, and corresponding distribution has $\cos^2 \phi_{pp}$ -dependence. This fundamental difference of the two mechanisms was observed also in other processes [30, 31, 34].

We have not discussed yet the influence of the off-shell effects in the matrix element on differential distributions. In the limit of real gluons the differential distributions are practically unchanged, so the corresponding off-shell effects are hard to observe taken the other theoretical uncertainties. Moreover, unlike for inclusive production case [38], shapes of differential distributions of Higgs CEP are not sensitive to the off-shell effects since they get averaged out effectively when the off-shell matrix element (5.5) is integrated over $\mathbf{q}_{0\perp}$ in

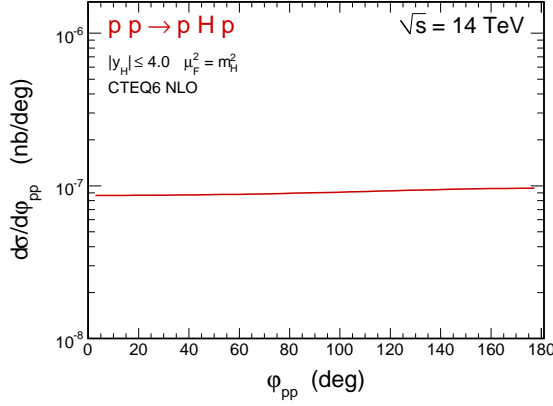


FIG. 21: Differential distribution in angle between outgoing protons for central exclusive Higgs boson production. CTEQ6 PDF was used in this calculation.

the diffractive amplitude (3.1).

C. Irreducible $b\bar{b}$ background for exclusive Higgs production

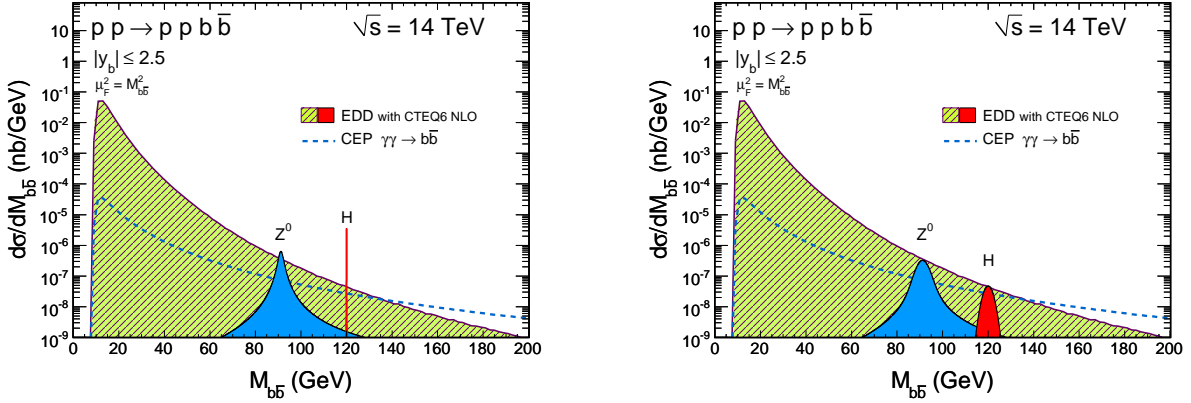


FIG. 22: The $b\bar{b}$ invariant mass distribution for $\sqrt{s} = 14$ TeV and for b and \bar{b} jets from Higgs decay in the rapidity interval $-2.5 < y_b < 2.5$ corresponding to the ATLAS detector. The absorption effects for the Higgs boson and the background were taken into account by multiplying cross section by the gap survival factor $\langle S^2 \rangle = 0.03$. The left panel shows purely theoretical predictions, while the right panel includes experimental effects due to experimental uncertainty in invariant mass measurement. The left peaks (bumps) correspond to the Z^0 contribution and the right ones to the Higgs contribution.

Now we turn to the analysis of the $b\bar{b}$ continuum as a background for the $b\bar{b}$ Higgs signal. In the left panel of Fig. 22 we show contributions of several CEP mechanisms to the $b\bar{b}$ quark invariant mass distribution. The diffractive $b\bar{b}$ and Higgs contributions were calculated for a selected (CTEQ6 [44]) collinear gluon distribution. The QED mechanism is also shown by the short-dashed line. Natural decay width, calculated as in Ref. [41], was assumed in

this calculation, see the sharp peak at $M_{b\bar{b}} = 120$ GeV (assumed arbitrarily for illustration) which is not excluded at present by the Higgs searches at LEP [47] and Tevatron [48].

As was already mentioned above, the phase space integrated cross section for the Higgs production, including absorption effects with $\langle S^2 \rangle = 0.03$ is less than 1 fb which is somewhat smaller than that predicted by the Durham group [4]. The main reason is different choice of the scale in the Sudakov form factor $\mu^2 = M_H^2$ instead of $\mu^2 = M_H^2/4$ as used by the Durham group. The first choice was advocated recently by theoretical studies in Ref. [37]. The result shown in Fig. 22 includes also the branching fraction $\text{BR}(H \rightarrow b\bar{b}) \approx 0.8$ and the rapidity restrictions. The second much broader Breit-Wigner type peak corresponds to the exclusive production of the Z^0 boson with the cross section calculated as in Ref. [49]. The exclusive cross section for $\sqrt{s} = 14$ TeV is 16.61 fb including absorption (28.71 fb without absorption effects). The branching fraction $\text{BR}(Z^0 \rightarrow b\bar{b}) \approx 0.15$ has been included in addition. In contrast to the Higgs case the absorption effects for the Z^0 production are much smaller [49]. The sharp peak corresponding to the Higgs boson clearly sticks above the background. In the above calculations we have assumed an ideal no-error measurement.

In reality the situation is, however, much worse as both protons and the b and \bar{b} jets are measured with a certain precision which automatically leads to a smearing of experimental distribution in $M_{b\bar{b}}$. Much better resolution can be obtained by measuring missing mass than from the direct measurement of heavy quark (antiquark) jet momenta. In the following in spite we will present distribution in $M_{b\bar{b}}$ (it will mean experimentally distribution in missing mass (M_{pp})). The two are identical when there are no errors on kinematical variables. While the smearing is negligible for the background, it leads to a significant modification of the Breit-Wigner peaks, especially of the sharp one for the Higgs boson. In the present paper the experimental effects are included in the simplest way by a convolution of the theoretical distributions and experimental resolution function

$$\frac{d\sigma^{exp}}{dM_{q\bar{q}}}(M_{q\bar{q}}) = \int d\mu \frac{d\sigma^{th}}{dM_{q\bar{q}}}(\mu) G(\mu - M_{q\bar{q}}) , \quad (6.1)$$

where the experimental resolution function is taken as the Gaussian function

$$G(x) = \frac{1}{\sqrt{2\pi}\sigma} \exp\left(-\frac{x^2}{2\sigma^2}\right) , \quad (6.2)$$

with $\sigma = 2$ GeV, which realistically represents the experimental situation [50, 51] and is determined mainly by the precision of measuring forward protons. In the right panel we show the invariant mass distribution when the invariant mass smearing is included. Now the bump corresponding to the Higgs boson is below the $b\bar{b}$ background. With the experimental resolution assumed above the identification of the Standard Model Higgs looks rather difficult. The situation for some scenarios beyond the Standard Model may be better [52].

Below we wish to discuss how to improve the situation by imposing extra cuts. Before we establish how to impose cuts let us consider first a few two-dimensional distributions which may help to come to the final solution.

Let us start from two-dimensional distributions in proton transverse momenta. In Fig. 23 we show distributions for the diffractive (left panel), photon-photon (middle panel) and for b and \bar{b} from the Higgs boson decay (right panel) contributions. In the case of the EDD and QED continua we are limited to a very restrictive range of invariant masses (117.6 GeV $< M_{b\bar{b}} < 122.4$ GeV) around the chosen Higgs mass in order to facilitate a comparison of the signal and background. While the distributions for the diffractive $b\bar{b}$ continuum and Higgs

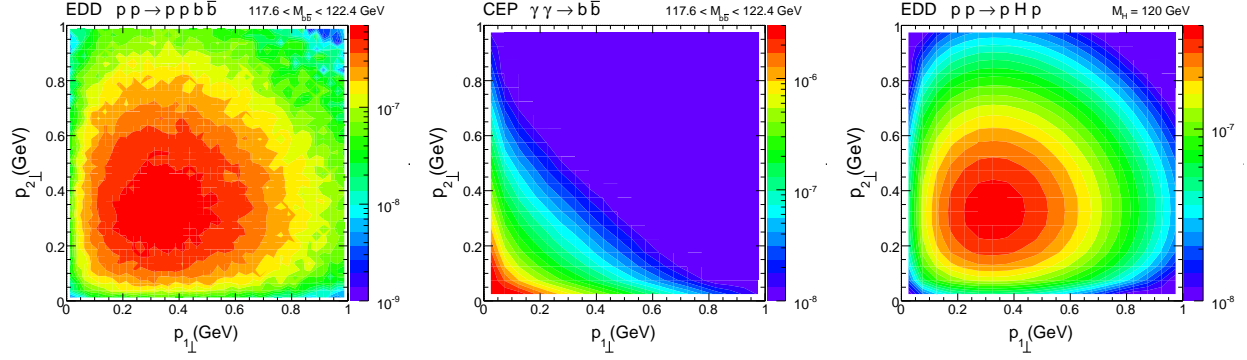


FIG. 23: Two-dimensional distributions in outgoing proton momenta $p_{1,2\perp}$ of the $b\bar{b}$ EDD (left) and QED (middle) continua integrated in the window $117.6 \text{ GeV} < M_{b\bar{b}} < 122.4 \text{ GeV}$ and Higgs CEP signal (right panel). Kinematical constraints are the same as in Fig. 22.

are rather similar the distribution for the photon-photon production differs considerably. While the first two ones are peaked at sizeable transverse momenta of about 0.3 GeV, the photon-photon contribution is peaked at extremely small proton transverse momenta due to photon propagators. Cutting off extremely small proton transverse momenta would allow to get rid of the photon-photon contribution to a large extent. It is not completely clear if this can be done easily experimentally. A Monte Carlo study including the experimental apparatus seems to be required.

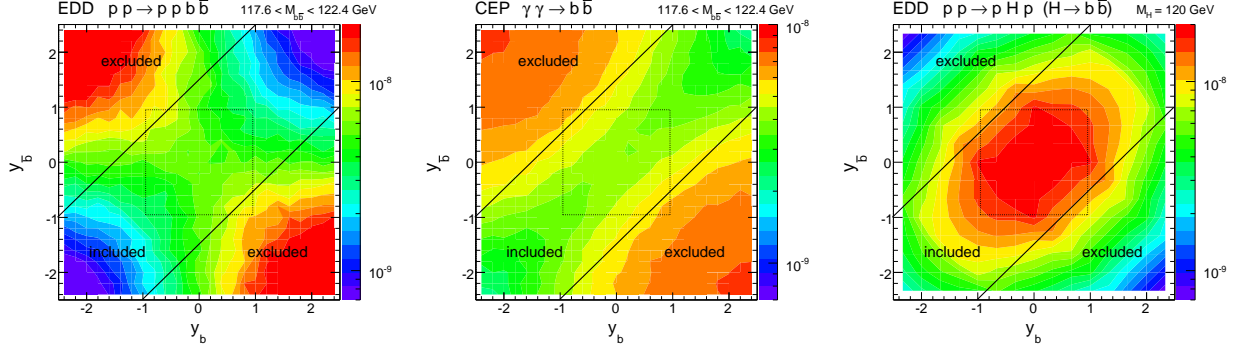


FIG. 24: Two-dimensional distributions in b and \bar{b} rapidities integrated in the window $117.6 \text{ GeV} < M_{b\bar{b}} < 122.4 \text{ GeV}$ for the diffractive QCD background (left panel), $\gamma^*\gamma^*$ contribution (middle panel) and Higgs CEP (right panel). Kinematical constraints are the same as in Fig. 22.

Next let us consider two-dimensional distributions in rapidities of the quark (y_b) and antiquark ($y_{\bar{b}}$). In Fig. 24, as in the previous case, we show separately distributions for diffractive continuum (left panel), photon-photon continuum (middle panel) and Higgs (right panel) contributions. The problem of the background subtraction looks here fairly favorable. In the case of the $b\bar{b}$ continuum production the cross section is maximal when quark and antiquark have opposite rapidities at the edges of the main detector (ATLAS, CMS). This is completely different for the Higgs contribution where the maximum occurs when $y_b, y_{\bar{b}} \sim 0$. Two windows suggesting how to get rid of the major part of the background are shown in Fig. 24: the square marked by the dashed line and the area between two parallel lines at 45° . The consequences of such cuts will be discussed in the following.

The situation can be also quantified in a one-dimensional plot in a function of the difference of the quark and antiquark rapidities (see Fig. 25). The distributions for the signal and background are very different. Imposing a cut on y_{diff} can significantly improve the signal-to-background ratio.

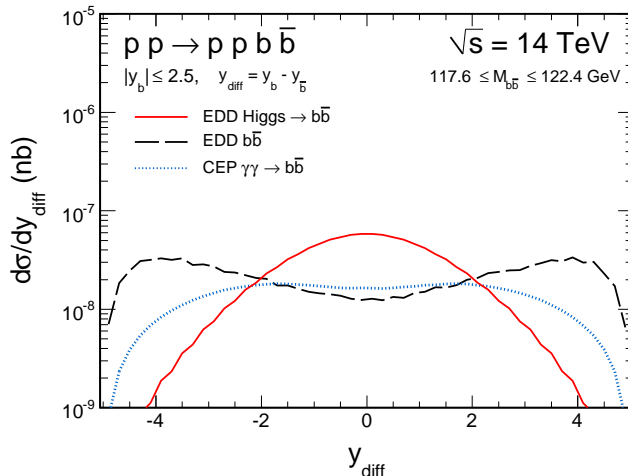


FIG. 25: Distribution in the difference of the quark and antiquark rapidities. Please note an extra cut on the $b\bar{b}$ invariant mass. Kinematical constraints are the same as in Fig. 22.

In Fig. 26 we show the distribution in the b -quark rapidity from Higgs decay and from a narrow region of $b\bar{b}$ invariant mass (given in the figure) for the diffractive $b\bar{b}$ and photon-photon components. While the Higgs contribution is concentrated at $y_b \sim 0$ the diffractive component has maxima at the edges of the central detector. The $\gamma\gamma$ contribution is rather flat across the range of the central detector. The different distributions in the b -quark rapidity of the different components suggest that limiting to midrapidities (i.e. not using the whole range of the detector) may help in improving the signal-to-background ratio.

Further useful handles to improve the situation are the jet transverse momenta which can be measured in the central detector. The importance of the cuts on the jet transverse momenta is illustrated in Fig. 27. Again we show the three components. While the signal (Higgs) contribution is peaked at the transverse momenta being half of the Higgs mass, the background contributions are flat or even have local maxima at low transverse momenta. Imposing therefore a lower cut on jet transverse momenta can again significantly improve the signal-to-background ratio without losing too much of the signal itself. Also, from experimental point of view the b (\bar{b}) jets can be well identified only above a certain cut on their transverse momenta.

Now we wish to quantify the effect of cuts on the $b\bar{b}$ invariant mass (missing mass experimentally) distribution. We shall impose cuts in order not to lose too much Higgs signal. In Fig. 28 we show the results for several scenarios (cuts). Here we omit the Z^0 contribution and concentrate solely on the Higgs signal. In the left upper corner we show result with the cut only on quark and antiquark rapidities (the square in Fig. 24) i.e. not making use of the whole coverage of the main LHC detectors. The signal is now above the diffractive background. We also show, by the thin dashed line, the photon-photon background which is only slightly smaller than the diffractive one. In the upper right corner we show the result for the cut on the quark and antiquark rapidity difference (see parallel thick solid lines in

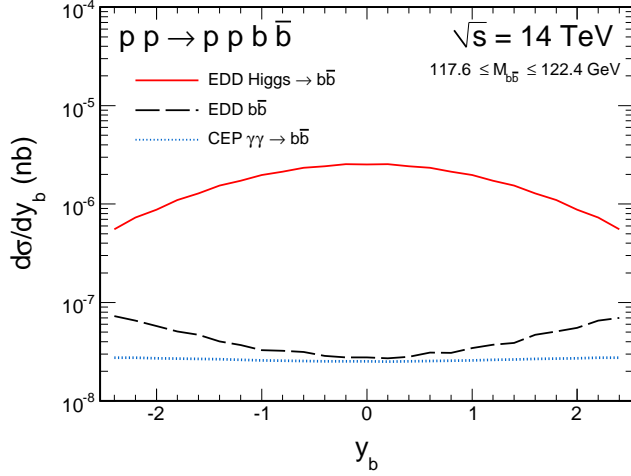


FIG. 26: Distribution in the quark/antiquark rapidity. Please note an extra cut on the $b\bar{b}$ invariant mass. Kinematical constraints are the same as in Fig. 22.

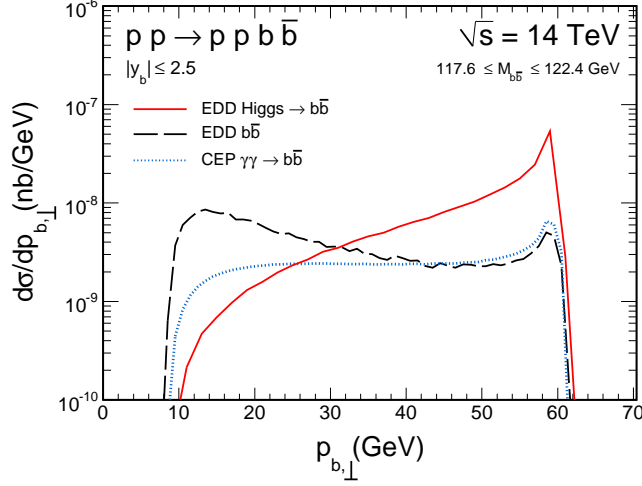


FIG. 27: Distribution in the jet transverse momentum for different components. Please note an extra cut on the $b\bar{b}$ invariant mass. Kinematical constraints are the same as in Fig. 22.

Fig. 24). The signal-to-background ratio is here similar, except that the cross sections are larger. In the lower left corner we show the situation with the lower cut on both quark and antiquark jets. The situation is similar as for the rapidity cuts. In order to eliminate the photon-photon contribution in the lower right corner we impose in addition a lower cut on proton transverse momenta. Now the signal clearly sticks above the background and the contribution of the photon-photon continuum is negligible. The cross section for the Higgs boson with the cuts is only 2-3 times smaller than that without the cuts.

The simultaneous inclusion of cuts on quark (antiquark) rapidities and transverse momenta does not improve further the signal-to-background ratio. It is enough in practice to include only one of them depending on experimental convenience. Why it is so is discussed in Fig. 29 where we show two-dimensional distributions in b -quark rapidity and transverse mo-

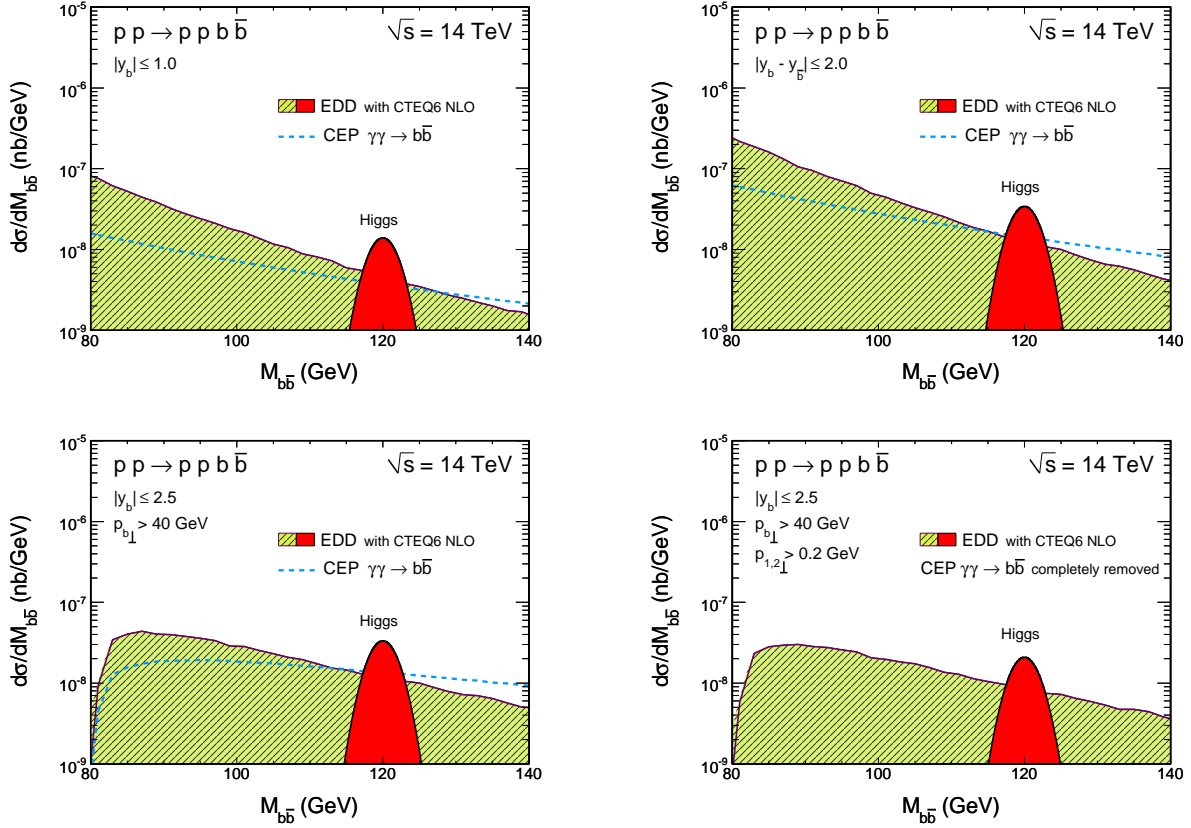


FIG. 28: The $b\bar{b}$ invariant mass distribution for $\sqrt{s} = 14$ TeV and for b and \bar{b} jets from Higgs decay with different limitations in the (anti)quark rapidity y_q , (anti)quark transverse momenta and outgoing proton momenta $p_{1,2\perp}$.

mentum for the $b\bar{b}$ invariant mass window around the Higgs mass. Here three well separated maxima are seen. One can extract them either by cuts on quark/antiquark rapidities or by cuts on quark/antiquark transverse momenta. This explains the equivalence of the cuts. Unlike the corresponding distribution not restricted to $M_{b\bar{b}}$ around Higgs, the distributions with the restriction have more complicated structure. While for the Higgs decay b -quarks are produced predominantly at midrapidities with transverse momenta $p_{\perp} \sim M_H/2$. The two-dimensional distributions for the diffractive continuum and the $\gamma^*\gamma^*$ fusion subprocess have three maxima: one as for the Higgs decay (smaller) and two other with much smaller transverse momenta and larger rapidities (bigger). For diffractive $b\bar{b}$ continuum the maxima at small p_{\perp} and large rapidities are much bigger. Identification of the maxima experimentally would be a confirmation of the present predictions. Imposing appropriate cuts in either rapidity or transverse momentum would allow to get rid of a large fraction of the diffractive background.

The equivalence of the cuts in rapidity and transverse momentum can be even better understood in the two-dimensional distribution in b -quark transverse momentum and the difference between quark and antiquark rapidities. Fig. 30 shows that for a fixed narrow interval of the $b\bar{b}$ invariant mass the rapidity difference between b and \bar{b} and the transverse momentum of b or \bar{b} are strongly correlated. This is of purely kinematical origin (see

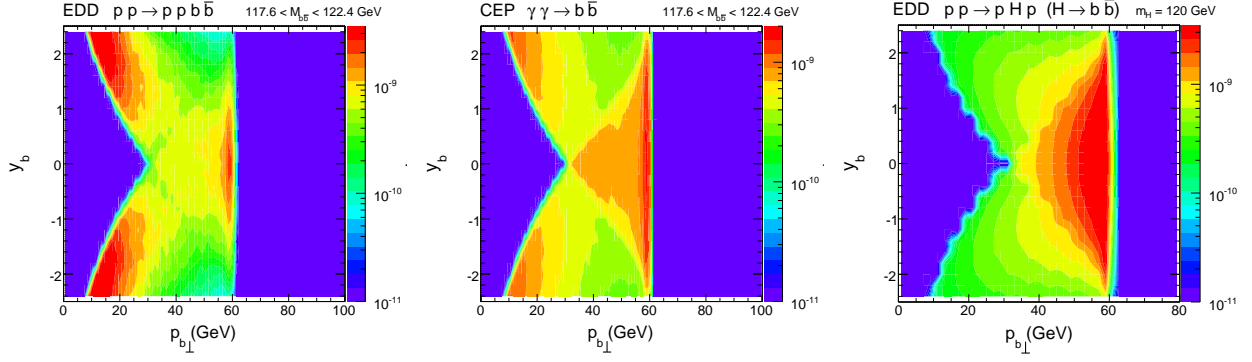


FIG. 29: Two-dimensional distribution in quark rapidity and quark transverse momentum for different mechanisms.

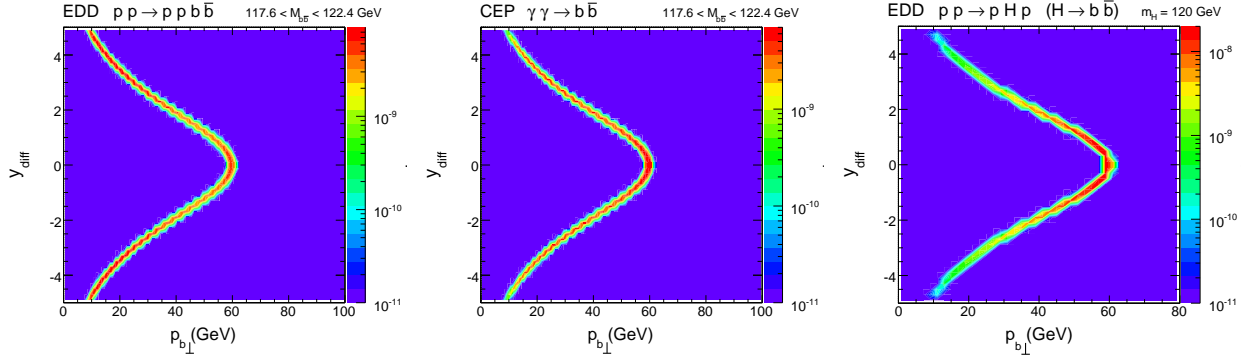


FIG. 30: Two-dimensional distribution in the quark-antiquark rapidity difference and quark transverse momentum.

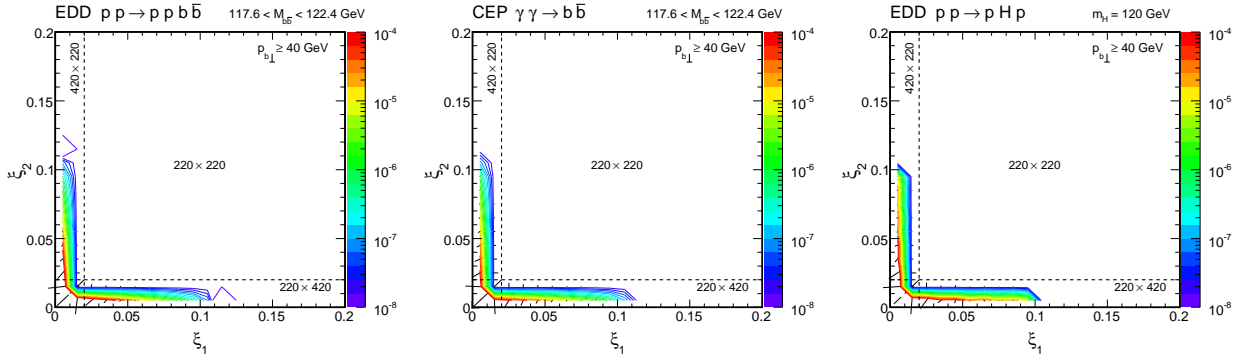


FIG. 31: The two-dimensional distributions in ξ_1 and ξ_2 for diffractive $b\bar{b}$ (left panel), $\gamma^*\gamma^* \rightarrow b\bar{b}$ (middle panel) and CEP of Higgs (right panel).

Eq. (3.17)) and demonstrates that imposing cuts on one of the two variables is equivalent and completely sufficient.

Above we have considered proton transverse momentum cuts. Can other outgoing proton variables be useful to improve the signal-to-background ratio? In Fig. 31 we show the distribution in proton longitudinal momentum fraction loses ξ_1 and ξ_2 defined as:

$$\xi_1 = 1 - x_F(\text{proton}_1), \quad \xi_2 = 1 - x_F(\text{proton}_2), \quad (6.3)$$

where x_F 's are the Feynman variables of outgoing protons 1 or 2. Only slightly different distributions for exclusive Higgs production (right panel), $b\bar{b}$ EDD (left panel) and QED $b\bar{b}$ (middle panel) continua can be seen. Imposing cuts on $\xi_1 > \xi_{cut}$ or $\xi_2 > \xi_{cut}$ could slightly improve the signal-to-background ratio but at the expense of severe deteriorating the statistics. In addition these cuts are quite correlated with the cuts on b -quark rapidities. By the dotted horizontal and vertical lines we have also marked limitations of the detectors planned at 220 and 420 meters from the collision point by the ATLAS and CMS collaborations. One can see that a pair of the 220 m detectors is not sufficient to measure Higgs boson. Both detectors on both sides are needed to measure most of the yield.

D. Other backgrounds

Our analysis in the previous subsection has been concentrated on the irreducible background only. Other contributions, although, in principle, reducible, can in practice be also rather troublesome [13]. The cross section for the gluonic dijets was found to be much larger than that for the $b\bar{b}$ jets [9]. If the gluon jets are misidentified as b -jets, which was estimated to be 1.3% for the ATLAS detector, they contribute to the Higgs background. In Ref. [13] the authors discuss in addition pile up events when the measured protons are not related to the exclusive Higgs production. Table 2 in their analysis presents detailed results for the issue. Inclusive double-pomeron processes [53] can also contribute to the background. Further analyses, especially for the Standard Model Higgs boson production, seem to be necessary to understand whether the Higgs boson can be identified in the exclusive production, perhaps not only in the $b\bar{b}$ decay channel. The present parton level analysis should be supplemented in the future by an additional analysis of $b\bar{b}$ jets by including a model of hadronization. Then standard jet algorithms could be imposed and the quality of the b and \bar{b} kinematical reconstruction could be studied in detail.

E. Some other remarks

We have not been interested here in the precise estimation of the cross section but rather in understanding the signal-to-background ratio which is of the major importance for the upcoming Higgs boson searches in exclusive mode at the LHC. Consequently, we have presented results with only one UGDF. This ratio is practically the same for other UGDFs. The absorption effects have been included here in a simple multiplicative form. They are expected to be the same both for the signal and the background, and thus are not affecting the ratio under consideration. The same gap survival factor has been used in both cases.

As was mentioned above, in the current analysis we do not take into account the next-to-leading order QCD corrections in hard subprocess parts in both the $b\bar{b}$ background and Higgs CEP. Calculations of such corrections in the hard subprocess $g^*g^* \rightarrow q\bar{q}$ within the k_\perp -factorization approach are rather cumbersome, and we postpone them for our future studies.

We have already analyzed the sensitivity of the results on the choice of UGDF. Different PDFs used to calculate UGDFs are defined in different range of factorization scales (gluon transverse momenta squared), some like CTEQ and MRST only for higher scales ($q_{\perp,min}^2 > 1 \text{ GeV}^2$), some like GRV and GJR for lower values ($q_{\perp,min}^2 > 0.4 \text{ GeV}^2$).

Let us analyze how important are the low gluon transverse momenta in evaluation of the cross section. In Fig. 32 we show how the total and differential in $M_{b\bar{b}}$ cross sections depend on the lowest value of the screening gluon transverse momentum squared used in evaluating the corresponding amplitude. There is much stronger dependence of the background than of the signal. This is caused by the specificity of matrix elements and the different three-body and four-body kinematics. It is interesting to note that at high lowest limit ($> 1 \text{ GeV}^2$) the cross section for different gluon distributions coincide. This shows that the differences of the cross section between different UGDFs come mainly from the region of relatively small values of the screening gluon transverse momenta. There is a stronger sensitivity on $q_{\perp, \min}^2$ for larger values of $b\bar{b}$ invariant mass (see the right panel in Fig. 32).

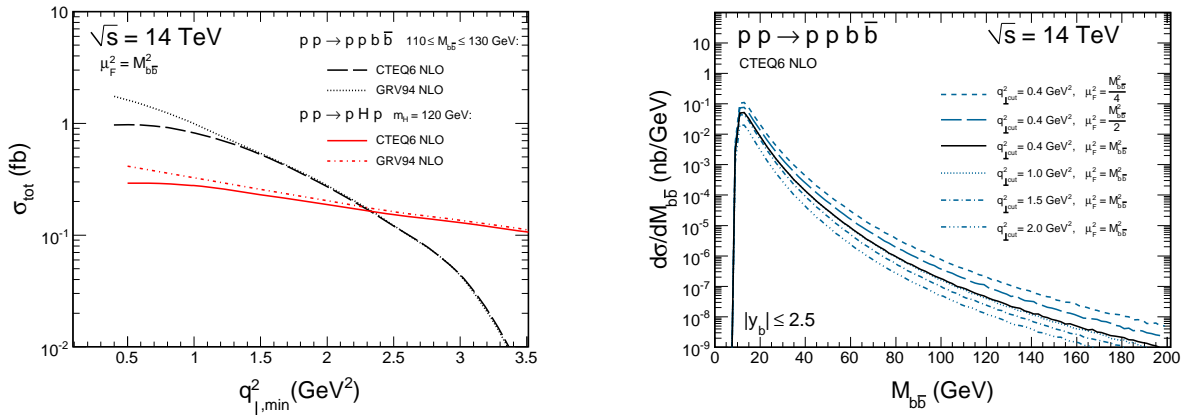


FIG. 32: Total $b\bar{b}$ and Higgs CEP cross section as a function of the lowest cut on the screening gluon transverse momentum scale (left panel) and the invariant mass distribution of the $b\bar{b}$ CEP for different values of the cut and different factorization scales (right panel).

In Fig. 33 we show the invariant mass distributions of exclusive $b\bar{b}$ pair production for $\lambda_b \lambda_{\bar{b}} = ++$ and $+-$ (anti)quark helicity contributions with the realistic lower cut $p_{b\perp} \geq 40 \text{ GeV}$ (so the high- p_{\perp} limit is concerned) on both quark and antiquark jets transverse momenta. The $+-$ contribution clearly dominates, however the $++$ contribution is not negligible, especially for very large invariant masses of the $b\bar{b}$ pair. Decreasing the cut-off on $p_{b\perp}$ relatively enlarges the $++$ contribution, making it important for low- p_{\perp} jets production.

VII. CONCLUSIONS

We have derived leading-order formula for the amplitude for EDD production of heavy quarks in the k_{\perp} -factorization approach. This formula takes into account both gluon virtualities (transverse momenta) as well as the quark masses neglected in earlier works in the literature. We have shown that corresponding $g^* g^* \rightarrow q\bar{q}$ vertex is gauge invariant. We have also discussed purely QED double-photon component.

Using the $2 \rightarrow 4$ diffractive amplitude we have calculated differential cross section for $c\bar{c}$ and $b\bar{b}$ central exclusive production (CEP) in (anti)quark rapidities, quark and proton transverse momenta, transverse momentum of the $q\bar{q}$ pair and in azimuthal angles between outgoing protons and quark dijets in the whole four-body phase space for the nominal

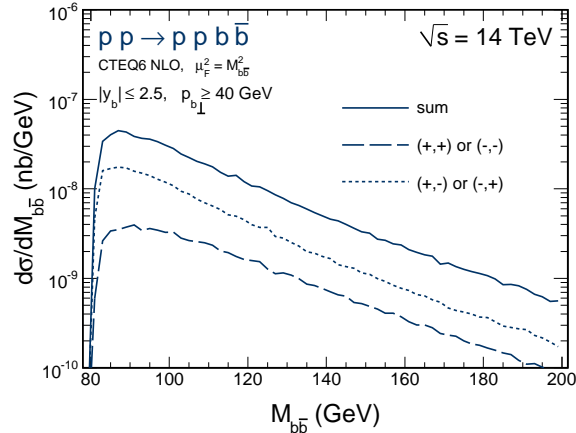


FIG. 33: Invariant mass distributions of EDD $b\bar{b}$ pair production for different (anti)quark helicities with the lower cut ($p_{b\perp} \geq 40$ GeV) on both quark and antiquark jets transverse momenta.

LHC energy $\sqrt{s} = 14$ TeV. Large cross sections have been found in contrast to previous expectations in the literature.

We have also discussed how the cross sections depends on quark masses. While at low quark-antiquark invariant masses the cross section for light quarks (u, d, s) is considerably larger than for heavy quarks (c, b) at large invariant masses the situation reverses. For instance, at invariant mass ~ 120 GeV (relevant for Higgs searches) it is the $b\bar{b}$ contribution which dominates. Since experimentally one can misidentify the other non- b quark jets as b -jets, our calculation shows that this is not so dangerous provided that the misidentification probability is not too high. The gluonic jets seems in this context more difficult because of much larger cross section [13].

We have also calculated differential distributions for exclusive Higgs production as well as for b and \bar{b} quarks (antiquarks) from the decay of the Higgs boson. We have used, for the first time in exclusive Higgs case, the vertex function which is consistently with the k_{\perp} -factorization approach i.e. takes into account the gluon virtualities in the hard subprocess vertex. We have discussed the role of the off-shell effects. In contrast to the exclusive χ_c production, the off-shell effects for Higgs boson are rather small and can be neglected given other sizeable theoretical uncertainties.

The $b\bar{b}$ EDD and QED continua constitute an irreducible background to the exclusive Higgs boson production. We have discussed in detail how to improve the signal-to-background ratio by imposing cuts in quark rapidities, proton transverse momenta, longitudinal momentum fraction of outgoing protons. The analysis in the $(y_b, y_{\bar{b}})$ -space is very useful to separate the two contributions as there they are located in quite different parts of this space. An optimal two-dimensional cut was proposed and the corresponding invariant mass distribution of the signal and background was presented.

VIII. ACKNOWLEDGMENTS

Useful discussions and helpful correspondence with Mike Albrow, Sergey Baranov, Rikard Enberg, Gunnar Ingelman, Igor Ivanov, Valery Khoze, Risto Orava, Andy Pilkington, Christophe Royon, Mikhail Ryskin and Oleg Teryaev are gratefully acknowledged. This

study was partially supported by the Carl Trygger Foundation and by the polish grant of MNiSW N N202 249235.

-
- [1] A. Schafer, O. Nachtmann and R. Schopf, Phys. Lett. B **249** (1990) 331
 - [2] A. Bialas and P.V. Landshoff, Phys. Lett. B **256** (1991) 540
 - [3] T. Aaltonen *et al.* [CDF Collaboration], Phys. Rev. D **77**, 052004 (2008) [arXiv:0712.0604 [hep-ex]];
A. A. Affolder *et al.* [CDF Collaboration], Phys. Rev. Lett. **88**, 151802 (2002) [arXiv:hep-ex/0109025];
A. A. Affolder *et al.* [CDF Collaboration], Phys. Rev. Lett. **85**, 4215 (2000).
 - [4] V. A. Khoze, A. D. Martin and M. G. Ryskin, Phys. Lett. B **401**, 330 (1997);
A. B. Kaidalov, V. A. Khoze, A. D. Martin and M. G. Ryskin, Eur. Phys. J. C **33**, 261 (2004).
 - [5] V. A. Khoze, M. G. Ryskin and A. D. Martin, Eur. Phys. J. C **64**, 361 (2009).
 - [6] A. De. Roeck *et al.*, Eur. Phys. J. **C25** (2002) 391;
S. Heinemeyer *et al.*, Eur. Phys. J. **C53** (2008) 231.
 - [7] A. G. Shuvaev, V. A. Khoze, A. D. Martin and M. G. Ryskin, Eur. Phys. J. C **56**, 467 (2008) [arXiv:0806.1447 [hep-ph]].
 - [8] M. G. Albrow, T. D. Coughlin and J. R. Forshaw, arXiv:1006.1289 [hep-ph];
J. L. Pinfold, arXiv:1006.0204 [hep-ph].
 - [9] J. R. Cudell, A. Dechambre, O. F. Hernandez and I. P. Ivanov, Eur. Phys. J. C **61**, 369 (2009).
 - [10] A. Dechambre, O. Kepka, C. Royon and R. Staszewski, Phys. Rev. D **83**, 054013 (2011) [arXiv:hep-ph/11011439].
 - [11] R. Maciuła, R. Pasechnik and A. Szczurek, Phys. Rev. D **83**, 054014 (2011) [arXiv:hep-ph/11011439].
 - [12] R. Maciuła, R. Pasechnik and A. Szczurek, Phys. Lett. B **685**, 165 (2010) [arXiv:0912.4345 [hep-ph]].
 - [13] B.E. Cox, F.K. Loebinger and A.D. Pilkington, JHEP 0710, 090 (2007).
 - [14] V. A. Khoze, A. D. Martin and M. G. Ryskin, Eur. Phys. J. C **19**, 477 (2001) [Erratum-ibid. C **20**, 599 (2001)] [arXiv:hep-ph/0011393].
 - [15] J. R. Cudell, A. Dechambre and O. F. Hernandez, arXiv:1011.3653 [hep-ph].
 - [16] S. Catani, M. Ciafaloni and F. Hautmann, Phys. Lett. B **242**, 97 (1990); Nucl. Phys. B **366**, 135 (1991);
J. C. Collins and R. K. Ellis, Nucl. Phys. B **360**, 3 (1991);
G. Camici and M. Ciafaloni, Phys. Lett. B **386**, 341 (1996); Nucl. Phys. B **496**, 305 (1997).
 - [17] P. Hagler, R. Kirschner, A. Schafer, L. Szymanowski and O. Teryaev, Phys. Rev. D **62**, 071502 (2000) [arXiv:hep-ph/0002077].
 - [18] P. Hagler, R. Kirschner, A. Schafer, L. Szymanowski and O. Teryaev, Phys. Rev. D **62**, 071502 (2000);
Ph. Hagler, R. Kirschner, A. Schafer, L. Szymanowski and O. V. Teryaev, Phys. Rev. D **63**, 077501 (2001) [arXiv:hep-ph/0008316]. P. Hagler, R. Kirschner, A. Schafer, L. Szymanowski and O. V. Teryaev, Phys. Rev. Lett. **86**, 1446 (2001).
 - [19] A.V. Lipatov, V.A. Saleev and N.P. Zotov, hep-ph/0112114;
S.P. Baranov, A.V. Lipatov and N.P. Zotov, Yad. Fiz. **67**, 856 (2004) [arXiv:hep-ph/0302171].
 - [20] V. S. Fadin and L. N. Lipatov, Nucl. Phys. B **477**, 767 (1996) [arXiv:hep-ph/9602287].

- [21] R. Enberg, G. Ingelman, A. Kissavos *et al.*, Phys. Rev. Lett. **89**, 081801 (2002). [arXiv:hep-ph/0203267].
- [22] P. Hagler, R. Kirschner, A. Schafer, L. Szymanowski and O. V. Teryaev, Phys. Rev. Lett. **86**, 1446 (2001) [arXiv:hep-ph/0004263].
- [23] J. R. Forshaw, arXiv:hep-ph/0508274.
- [24] I.P. Ivanov, N.N. Nikolaev, Phys. Rev. D **65**, 054004 (2002).
- [25] R. Maciuła, R. Pasechnik and A. Szczurek, work in progress.
- [26] V. A. Khoze, A. D. Martin and M. G. Ryskin, Eur. Phys. J. C **18**, 167 (2000) [arXiv:hep-ph/0007359].
- [27] M. A. Kimber, A. D. Martin and M. G. Ryskin, Phys. Rev. D **63**, 114027 (2001) [arXiv:hep-ph/0101348];
- [28] A. D. Martin and M. G. Ryskin, Phys. Rev. D **64**, 094017 (2001) [arXiv:hep-ph/0107149].
- [29] A. G. Shuvaev, K. J. Golec-Biernat, A. D. Martin and M. G. Ryskin, Phys. Rev. D **60**, 014015 (1999) [arXiv:hep-ph/9902410].
- [30] A. Szczurek, R. S. Pasechnik and O. V. Teryaev, Phys. Rev. D **75**, 054021 (2007) [arXiv:hep-ph/0608302].
- [31] R. S. Pasechnik, A. Szczurek and O. V. Teryaev, Phys. Rev. D **78**, 014007 (2008) [arXiv:0709.0857 [hep-ph]].
- [32] B. Pire, J. Soffer and O. Teryaev, Eur. Phys. J. C **8**, 103 (1999) [arXiv:hep-ph/9804284].
- [33] X. Artru, M. Elchikh, J. M. Richard, J. Soffer and O. V. Teryaev, Phys. Rept. **470**, 1 (2009) [arXiv:0802.0164 [hep-ph]].
- [34] R. S. Pasechnik, A. Szczurek and O. V. Teryaev, Phys. Lett. B **680**, 62 (2009);
R. S. Pasechnik, A. Szczurek and O. V. Teryaev, Phys. Rev. D **81**, 034024 (2010).
- [35] R. Pasechnik, R. Enberg and G. Ingelman, Phys. Rev. D **82**, 054036 (2010) [arXiv:hep-ph/1005.3399];
R. Pasechnik, R. Enberg and G. Ingelman, Phys. Lett. B **695**, 189 (2011) [arXiv:hep-ph/1004.2912].
- [36] A. B. Kaidalov, V. A. Khoze, A. D. Martin and M. G. Ryskin, Eur. Phys. J. C **31**, 387 (2003) [arXiv:hep-ph/0307064].
- [37] T. D. Coughlin and J. R. Forshaw, JHEP **1001**, 121 (2010) [arXiv:0912.3280 [hep-ph]].
- [38] R. S. Pasechnik, O. V. Teryaev and A. Szczurek, Eur. Phys. J. C **47**, 429 (2006).
- [39] F. Hautmann, Phys. Lett. B **535**, 159 (2002) [arXiv:hep-ph/0203140].
- [40] V. A. Khoze, A. D. Martin and M. G. Ryskin, Eur. Phys. J. C **23**, 311 (2002) [arXiv:0111.078 [hep-ph]].
- [41] G. Passarino, Nucl. Phys. B **488**, 3 (1997).
- [42] M. Glück, E. Reya and A. Vogt, Z. Phys. C **67**, 433 (1995).
- [43] M. Glück, D. Jimenez-Delgado, E. Reya, Eur. Phys. J. C **53**, 355 (2008).
- [44] J. Pumplin, D. R. Stump, J. Huston, H. L. Lai, P. M. Nadolsky and W. K. Tung, JHEP **0207**, 012 (2002).
- [45] A. D. Martin, W. J. Stirling, R. S. Thorne and G. Watt, Eur. Phys. J. C **63**, 189 (2009). [arXiv:0901.0002 [hep-ph]].
- [46] A. Kupco, R.B. Peschanski and C. Royon, Phys. Lett. B **606**, 139 (2005) [arXiv:0407222 [hep-ph]].
- [47] ALEPH Collaboration, DELPHI Collaboration, L3 Collaboration, OPAL Collaboration, SLD Collaboration, LEP Electroweak Working Group, SLD Electroweak Group, SLD Heavy Flavour Group, Phys. Rept. **427**, 257 (2006);

- ALEPH Collaboration, CDF Collaboration, D0 Collaboration, DELPHI Collaboration, L3 Collaboration, OPAL Collaboration, SLD Collaboration, LEP Electroweak Working Group, Tevatron Electroweak Working Group, SLD electroweak heavy flavour groups, FERMILAB-TM-2446-E, CERN-PH-EP-2009-XXX, arXiv:0911.2604 [hep-ex].
- [48] A. Dominguez *et al* [CDF and D0 Collaborations], AIP Conf. Proc. **1182**, 138 (2009); CDF Collaboration, D0 Collaboration, Tevatron New Physics and Higgs Working Group, FERMILAB-CONF-09-557-E, arXiv:0911.3930 [hep-ex].
- [49] A. Cisek, W. Schäfer and A. Szczurek, Phys. Rev. D **80** 074013 (2009).
- [50] A. Pilkington, private communication.
- [51] Ch. Royon, private communication.
- [52] R. Maciuła, R. Pasechnik and A. Szczurek, work in progress.
- [53] M. Boonekamp, R. Peschanski and C. Royon, Phys. Rev. Lett. **87** 251806 (2001).

